1 **Combined effects of stream hydrology and land use on basin-scale hyporheic zone**

2 **denitrification in the Columbia River Basin**

3 Kyongho Son[1], Yilin Fang[1], Jesus D. Gomez-Velez[2,3], Kyuhyun Byun[4], and Xingyuan Chen[1]

4 [1]Pacific Northwest National Laboratory, Richland, Washington, USA; [2]Department of Civil and

5 Environmental Engineering, Vanderbilt University, Nashville, Tennessee, USA; [3]Climate

6 Change Science Institute & Environmental Sciences Division, Oak Ridge National Laboratory,

7 Oak Ridge, TN, USA; [4]Department of Environmental Engineering, Incheon National University,

8 Incheon, 22012, South Korea

9 **Key Points**

10 • Hyporheic exchange flux controls the spatial variation of denitrification across reaches

11 with different sizes and land uses.

12 • The combination of hyporheic exchange flux and stream DOC explains the differences

13 in denitrification for different land use streams.

14 • D50, stream slope, precipitation, evapotranspiration, and shrub area can explain most of

15 the spatial variability in denitrification.

16

17 Corresponding author: Kyongho Son, kyongho.son@pnnl.gov

24

25 **Abstract**

26 Denitrification in the hyporheic zone (HZ) of river corridors is crucial to removing excess

27 nitrogen in rivers from anthropogenic activities. However, previous modeling studies of the

28 effectiveness of river corridors in removing excess nitrogen via denitrification were often limited

29 to the reach-scale and low-order stream watersheds. We developed a basin-scale river corridor

30 model for the Columbia River Basin with random forest models to identify the dominant factors

31 associated with the spatial variation of HZ denitrification. Our modeling results suggest that the

32 combined effects of hydrologic variability in reaches and substrate availability influenced by

33 land use are associated with the spatial variability of modeled HZ denitrification at the basin

34 scale. Hyporheic exchange flux can explain most of spatial variation of denitrification amounts

35 in reaches of different sizes, while among the reaches affected by different land uses, the

36 combination of hyporheic exchange flux and stream dissolved organic carbon (DOC)

37 concentration can explain the denitrification differences. Also, we can generalize that the most

38 influential watershed and channel variables controlling denitrification variation are channel

39 morphology parameters (median grain size (D50), stream slope), climate (annual precipitation

40 and evapotranspiration), and stream DOC-related parameters (percent of shrub area). The

41 modeling framework in our study can serve as a valuable tool to identify the limiting factors in

42 removing excess nitrogen pollution in large river basins where direct measurement is often

43 infeasible.

44 **Keywords: hyporheic zone, denitrification modeling, random forest model, stream size, and**

45 **land use**

46

1. Introduction

Air pollution, fertilizer use in agricultural lands, and wastewater effluents and polluted stormwater runoff from urban lands often result in stream nitrogen pollution, which also increases the frequency of eutrophication, hypoxia, and harmful algal blooms in lakes and estuaries (Boyer et al., 2006; Frei et al., 2020; Le Moal et al., 2019; Pinay et al., 2015, 2018). To lessen stream nitrogen pollution, we can reduce the nutrient loading or increase the nitrogen removal activity through in-stream nitrogen decay or the denitrification process in river corridors or soils (Frei et al., 2020; Pinay et al., 2018). Generally, denitrification is the most effective way to transform inorganic forms of excess nitrogen to a gas form (N_2) emitted to the atmosphere (Boyer et al., 2006). However, with the importance of denitrification, there are still considerable uncertainties in modeling denitrification in terrestrial and aquatic systems (Groffman, Butterbach-Bahl, et al., 2009) due to the high spatial and temporal heterogeneity of key controlling factors (oxygen, nitrate, carbon and pH, temperature, etc.). Therefore, quantifying denitrification in river corridors with varying spatial and temporal scales is challenging, especially for the hyporheic zone (HZ) at large spatial scales (Lee-Cullin et al., 2018).

Denitrification in the HZ varies with local conditions, including substrate availability (e.g., dissolved organic carbon (DOC), dissolved oxygen (DO) and nitrate), sediment properties (e.g., grain size), and hydrologic exchange flux/residence time (Kreiling et al., 2019; Seitzinger et al., 2006; Fork and Heffernan 2014; Findlay et al., 2011; Boyer et al., 2006; Tank et al., 2008; Zarnetske et al., 2015). Large-scale drivers, including land use/cover and climate, can alter local conditions, for example agricultural and urban watersheds tend to have higher potential denitrification than undisturbed watersheds (Mulholland et al., 2008). However, the critical controlling factors may change with scale and land use. Kreiling et al. (2019) showed that stream nitrate availability is a crucial variable that controls the spatial variation of denitrification in the Fox River watershed in Wisconsin, a mixed land use landscape. Baker and Vervier (2004) showed that the concentration of low molecular weight organic acids is the best predictor for explaining spatiotemporal patterns of denitrification variables. Even though we know that the combined effects of hydrologic variability and substrate concentration control denitrification, it is unclear which factors become dominant and under what conditions. Bardini et al. (2012) used numerical modeling to demonstrate that streambeds can alternate between net nitrification and net denitrification states by varying physical and chemical constraints. In particular, their

78   numerical simulation study showed that hydrologic variability is more important than reaction

79   substrate availability (DOC and NO_3^-) to drive such changes in streambed biogeochemical

80   transformations. The relative importance of hydrologic and substrate variables may vary with

81   land use and stream size; for example, a study by Myers (2008) found that, for a selected number

82   of sites, denitrification in agricultural streams is limited by hyporheic exchange flux, while in

83   forest streams it is limited by substrate availability.

84   Previous denitrification studies are often limited to reach scale to lower order streams and

85   have emphasized the importance of the role of lower order streams in denitrification (Alexander

86   et al., 2000, 2007; Gomez-Velez et al., 2015; Tank et al., 2008). Due to the higher ratio of

87   benthic surface-to-water volume and nutrient loading in lower order streams, denitrification's

88   efficiency in lower order streams is higher than that of higher order streams (Wollheim, 2016).

89   This result may be relevant to the empirical studies' sample bias, as Tank et al. (2008) pointed

90   out in their meta-analysis that most stream nutrient uptake studies for NH_4^+ and NO_3^- were

91   conducted at streams with less than 200 l/s. Using a pulse tracer test method, Tank et al. (2008)

92   also demonstrated that larger streams in the Upper Snake River (7th order and 12,000 l/s) have

93   higher inorganic nitrogen uptake (NH_4^+ and NO_3^-) than smaller streams. Ensign and Doyle (2006)

94   analyzed the results of nutrient spiraling experiments spanning from 1st order to 5th order

95   streams. They found that the cumulative uptake rate of NO_3^- increases with stream orders.

96   Similarly, a recent modeling study showed the potentially important role played by larger rivers

97   in removing excess nitrogen (Wollheim, 2016). Therefore, it is vital to investigate further how

98   stream size affects hyporheic exchange processes (Gomez-Velez & Harvey, 2014; Hotchkiss et

99   al., 2015; Tank et al., 2008; Wollheim et al., 2006). Furthermore, many previous modeling

100   studies did not separate the role of HZ denitrification from the whole-stream denitrification

101   (Alexander et al., 2000, 2007, 2009; Schmadel et al., 2021; Wollheim, 2016), so studying HZ

102   denitrification along streams with varying hydrologic and biogeochemical conditions is critical.

103   Previously, few basin-scale numerical models have been developed to simulate the role of

104   river corridors in removing excess nitrogen from streams and rivers (Alexander et al., 2007,

105   2009; Curie et al., 2011; Fang et al., 2020; Gomez-Velez & Harvey, 2014). However, most of the

106   basin-scale models are based on empirical reaction models, or the reaction parameters are

107   estimated by fitting the empirical data (Alexander et al., 2000, 2009; Wise et al., 2019). For

108   example, the Networks with Exchange and Subsurface Storage (NEXSS) used an empirical

109   hydrogeomorphic model and a suite of hydraulic and groundwater models to compute the

110   hyporheic exchange flux and residence time along river networks (Gomez-Velez et al., 2015;

111   Gomez-Velez & Harvey, 2014). The NEXSS model determines potential denitrification based on

112   the ratio of computed Damkohler number and river turnover length. However, this potential

113   denitrification does not consider the limitation of substrate availability in the denitrification rate.

114   The SPAtially Referenced Regressions on Watershed attributes (SPARROW) model was used to

115   estimate in-stream removal of nitrogen in the Mississippi River Basin (Alexander et al., 2000,

116   2007) and the Pacific regions (Wise et al., 2019). In-stream removal of nitrogen was estimated

117   by fitting the model parameters with the measured mean nitrogen fluxes without considering

118   explicitly nitrogen processes in streams. Also, this model does not separate the nitrogen removal

119   from the water column and HZ. Thus, the sole contribution of the nitrogen removal from the HZ

120   cannot be quantified. An integrated surface and subsurface model (Amanzi-ATS) was developed

121   to compute aerobic respiration and denitrification in the HZ at the watershed scale (Jan et al.,

122   2021), but this study is still limited to demonstrating the capability of the watershed model to

123   simulate the HZ processes and their impacts on stream water quality in an agriculture-dominant

124   watershed. Applying the ATS model in a large river basin and understanding the important

125   factors associated with denitrification is computationally too expensive.

126   On the other hand, Fang et al. (2020) developed SWAT-MRMT-R, a model that couples the

127   watershed water quality model, Soil and Water Assessment Tool (SWAT), with the reaction

128   module from a flow and reactive transport code (PFLOTRAN). It can compute aerobic

129   respiration and denitrification in the HZ. The model was successfully tested in the upper

130   Columbia–Priest Rapids watershed in the Columbia River Basin (CRB). It showed that the

131   spatial variation of HZ denitrification depends on a combination of varying hyporheic exchange

132   and source locations of nitrate.

133   While physically based numerical models can represent explicit mechanisms and simulate

134   HZ denitrification at varying spatial and temporal scales, these models are computationally

135   expensive (Ren et al., 2021) and require various data sources for model calibration (Chen et al.,

136   2021). As an alternative, machine learning approaches show high performance with limited data

137   and capture complex relationships between inputs and outputs (Mori et al., 2019). In some cases,

138   both approaches can be combined to gain further insight and predictability. For example, the

139 model can be used to reveal the dominant process or features through variable importance

140 analysis (Ren et al., 2020, 2021; Ward et al., 2022).

141   In this study, we adopted the reaction network model from the SWAT-MRMT-R to study

142 the role of the HZ in removing excess nitrogen at the basin scale. We applied this modeling

143 framework to the CRB, covering a wide range of channel sizes and land uses. A detailed

144 description follows in the methodology section. We used the CRB as a testbed to study the

145 spatial variation of HZ denitrification at the basin scale. The developed basin-scale HZ river

146 corridor model (RCM) aims to quantify the spatial variation of HZ denitrification across the

147 reaches of the CRB. A random forest model, a machine learning approach, is then used to

148 identify the dominant factors associated with the spatial variation of HZ denitrification at the

149 basin scale (Figure 1). Specifically, we ask two questions:

150   1. What dominant variables explain the spatial variation of HZ denitrification in the CRB?

151   We hypothesized that (i) the relative importance of hydrologic variability and substrate

152   availability can control the spatial variation of HZ denitrification and (ii) their

153   significance may change with stream size and dominant land use. We built random forest

154   models with key input variables and modeled denitrification results to test this

155   hypothesis. With this approach, we identify the variables that can better explain the

156   spatial variation of modeled denitrification across streams with different sizes and land

157   uses.

158   2. Which watershed/stream characteristics can better explain the spatial variation of HZ

159   denitrification in the CRB? We extended our efforts to develop another random forest

160   model to capture the modeled denitrification in the CRB with publicly available

161   watershed and stream characteristic data. This random forest model can generalize which

162   watershed/stream characteristics can better explain the spatial variation of the HZ

163   denitrification in the CRB.

164

165   **2. Methodology**

166   This study uses the RCM to explore the spatial patterns of HZ denitrification across reaches

167 with different sizes and land use in the CRB. Our main objective is to use the RCM as a virtual

168 reality model, and the machine-learning models as surrogates that encapsulate the complexities

169 of the physics-based model while identifying the importance of different variables that are not

170   evident in the model conceptualization. We do not include a direct comparison of the modeled

171   HZ denitrification and measurements; however, we believe that the RCM can capture the overall

172   spatial patterns of the HZ denitrification because the model inputs and its reaction networks are

173   based on well-established theory (Fang, et al., 2020; X. Song et al., 2018) and a physical-based

174   model (Gomez-Velez et al., 2015; Gomez-Velez & Harvey, 2014) or measurements (Li et al.,

175   2017). The combination of the model-based predictions and a machine-learning approach (e.g.,

176   random forest) is used to improve our understanding of what variables of the model are

177   associated with spatial patterns of the modeled denitrification across reaches with different sizes

178   and land uses, and to develop a proxy model using measurable variables to reproduce the

179   simulated patterns.

180   **2.1 Columbia River Basin**

181   The study site is the CRB (Figure 2), a large transboundary river basin with approximately

182   5,230 m of relief and a drainage area of 620,000 km^2. Here, we focus on 570,413km^2 of the basin

183   within the continental United States. We selected this fraction of the basin due to data

184   availability. For example, only the U.S. CRB has data from the National Hydrography Dataset

185   (NHD) Plus v2, and our spatial template and the hyporheic exchange and residence time

186   estimates are only available for this region.

187   The CRB can be divided into nine sub-river basins: (1) Lower Columbia; (2) Middle

188   Columbia; (3) Upper Columbia; (4) Lower Snake; (5) Middle Snake; (6) Upper Snake; (7)

189   Kootenai-Pend Oreille-Spokane; (8) Willamette; and (9) Yakima River (Figure 1b). The basin

190   expands various climatic and land use/cover classes. For example, western Washington and

191   Oregon have humid continental climate; eastern Washington and Oregon, and Idaho have a semi-

192   arid steep climate; and the Cascade Range in Washington and Oregon, and the Rocky Mountains

193   in Idaho, Montana, and Wyoming have an alpine climate. The variations in climate are reflected

194   in the annual precipitation, which ranges from 158 to 5,230 mm (based on 30 years of

195   normalized PRISM data), and the mean annual temperature, which ranges from -3 to 12°C. The

196   seasonal pattern of precipitation is very consistent with winter precipitation being dominant.

197   Higher elevations are dominated by precipitation in the phase of snow, while in lower elevation

198   regions precipitation falls primarily as rain. Major land use/cover (Figure 1c) is composed of

199 33.7% forest land (33% evergreen forest and about 0.3 and 0.4% deciduous forest and mixed

200 forest), 33% of shrub lands, 12% agriculture lands (10% croplands and 2% hay and pasture), and

201 2.3% urban lands.

2.2 Basin-scale hyporheic zone river corridor model

203 The RCM used in this study is a simplified, spatially resolved, basin-scale model that couples

204 carbon and nitrogen dynamics. We focus on simulating the spatial variation of HZ denitrification

205 in the CRB (Figure A1). The model adopted the reaction network model from SWAT-MRMT-R

206 (Fang, et al., 2020). Three microbially driven reactions, including two-step denitrification and

207 aerobic respiration, are considered within the HZ (Table A1). Note that this model only simulates

208 the HZ denitrification in the stream sediments without accounting for the denitrification process

209 in water column. The detailed equations and descriptions are found in the appendix and Fang et

210 al. (2020). Key model inputs are stream substrate concentrations (DOC, DO, and NO_3^-), and HZ

211 exchange flux and residence time. The model computes at hourly time steps to capture the fast

212 reaction time characterizing the biogeochemical processes represented in Tables A1 and A2, but

213 the model inputs are constant over time; thus, we consider that the modeled HZ denitrification

214 represents long-term averaged conditions. The RCM computes mean annual NO_3^- removal

215 (kgN/day) at the scale of the NHDPLUS stream reaches over the simulation periods and scales it

216 by stream surface area (m^2), using two parameters (channel width and length). The stream length

217 and width was derived from the NHDPLUS database (Schwarz et al., 2018), and the power

218 relationship between measurement of instantaneous flow and bankfull width and NHD

219 cumulative drainage area (Gomez-Velez et al., 2015), respectively. The model separately

220 calculates the NO_3^- removal amounts via vertical and lateral hyporheic exchange. To test the

221 variation of mean annual NO_3^- removal amounts between years, we ran the model over 10 years

222 and found that after 2 years of simulation, the removal amounts reached a dynamic steady state

223 (Figure S1). For our modeling analysis, the 2nd year simulation results were used.

224 Among model inputs, the exchange rate and residence time between stream and HZ were

225 estimated using NEXSS (Gomez-Velez and Harvey 2014). The NEXSS model coupled empirical

226 geomorphologic models with a suite of existing physical hyporheic exchange flux models; for

227 example, NEXSS estimates the values of bankfull channel with discharge, median grain size

228 (D50), channel slope, sinuosity, and regional head gradients along the NHDPLUS stream

229 networks. In addition, physical hyporheic exchange modeling is used to predict the average

230 hyporheic exchange flux, residence time distribution, and median residence time in the vertical

231 and lateral direction. Vertical hyporheic flux represents exchange between channel water and

232 bedforms, while lateral exchange flux represents exchange between channel water and river bars

233 and meander banks.

234   Stream substrate concentrations, including DOC, DO and NO_3^- (Figure 3), are determined via

235 empirical regression-based estimates or the output of the SPARROW 2012. For the stream NO_3^-

236 concentration, we used results of the 2012 SPARROW model

237 (https://www.sciencebase.gov/catalog/item/5d407318e4b01d82ce8d9b3c). SPARROW is a

238 statistical regression model and has been used to identify key pollutant sources and determine the

239 role of in-stream process in removing nutrients at the regional scale (Alexander et al., 2007;

240 Wise et al., 2019). SPARROW outputs include mean annual streamflow, total nitrogen loading,

241 total phosphorous loading, and suspended solid loading at the NHDPLUS stream reaches. Since

242 our RCM requires stream nitrate concentration, we calculated the mean annual total nitrate

243 concentration by dividing the total nitrogen mean annual loading by the mean annual streamflow

244 estimates and multiplying by the ratio of NO_3^- to total nitrogen concentration. The ratio was

245 computed based on the measured NO_3^- and total nitrogen concentrations at the U.S. Geological

246 Survey gauge stations in the CRB. To compute stream NO_3^- concentration, the ratio of stream

247 nitrate concentration to the total stream nitrogen was multiplied by the total nitrogen

248 concentration. Detailed analysis is included in the supporting information.

249   For stream DOC and DO concentrations, we developed multilinear regression models based

250 on the NHD stream database (Schwarz et al., 2018) and the measured stream DOC/DO

251 concentrations at the gauging stations in the CRB. The developed stream DOC concentration

252 model is a function of the percentage of basin/catchment shrub areas (tshrub and logshrub), a

253 basin agriculture area (logtargc) (stream DOC = -0.03 (tshrub) + 0.45 (logtargc) – 0.12

254 (logshrub) + 3.15). Reaches with higher agriculture lands tend to have higher DOC

255 concentrations, but those with higher shrub lands tend to have lower DOC concentrations. The

256 developed stream DO concentration model is a function of basin soil bulk density

257 (TOT_BDAVE), basin topographic wetness index (TOT_TWI), basin drainage area

258 (TOT_BASIN), and catchment dam storage (logCAT_NID) (stream DO = -2.85

259 (TOT_BDAVAE) – 0.49 (TOT_TWI) + 0.31 (logTOT_BASIN_AREA) + 0.12 (logCAT_NID).

260   The reaches with higher drainage area and dam storage tend to have higher DO concentrations,

261   but those with higher bulk density soil and wetted areas tend to have lower DO concentrations.

262   The detailed procedures of building multiple regression models for spatial DOC/DO mean

263   concentrations are included in the supporting information.

264   **2.3 Spatial variation of modeled hyporheic zone denitrification**

265   2.3.1   Reach- and basin-scale HZ denitrification within the CRB

266   We quantified the spatial variability of mean annual NO_3^- removal amount at the NHDPLUS

267   reach- and sub-basin scale. We explored how the spatial patterns change with channel size and

268   land use. This study classified the channel sizes in the three groups based on Strahler's stream

269   ordering system: (1) small streams (1st–3rd), (2) medium rivers (4th–6th), and (3) large rivers (7th–

270   12th). While the largest stream/river in the CRB is 9th order, the large rivers include the 7th to 9th

271   orders in our analysis. To determine the dominant land use for each reach, we calculated the

272   percentage of each land use (forest, urban, agriculture, and shrub) within the total upstream

273   routed accumulated area. If the percentage of the drainage area for each land use type is larger

274   than 80%, we assigned that type as the dominant land use. National Land Cover Database 2001

275   land cover (https://www.mrlc.gov/) was used to calculate the percentage of each land cover. To

276   simplify the classification, forest land use includes mixed, deciduous, and evergreen forest types;

277   urban land use includes developed open spaces and developed low/medium/high density area;

278   agriculture land use includes pasture/hay and cultivated crop areas; and shrub land use includes

279   dwarf scrub and shrub/scrub. We quantified the difference in the mean daily HZ NO_3^- removal

280   amounts in the reaches with different sizes (small, medium, and large streams/rivers) and

281   different land uses (forest, urban, agriculture, and shrub). The significance of the effect of land

282   use and reach size on the mean daily HZ NO_3^- removal amount was tested using the Kruskal-

283   Wallis test.

284   2.3.2   Sensitivity of HZ denitrification to substrate concentrations

285   The stream substrate concentrations at the NHDPLUS reach scale are estimated via the

286   existing SPARROW model or measured stream DOC/DO concentration; therefore, their

287   estimates are expected to have a high uncertainty that can affect the modeling results. To

288   quantify the impact of substrate concentration on the model estimates, we create four seasonal

289   stream DOC and DO concentration maps, and evaluate how the modeled NO_3^- removal amount

290   changes with different seasonal concentrations. The detailed descriptions of the seasonal

291   substrate concentrations are included in the supporting information. We also apply the maximum

292   and minimum of substrate concentrations and evaluate which limits the denitrification process in

293   the reaches across the different sizes and land uses. For example, the maximum value of

294   predicted DOC and NO_3^- and minimum value of predicted DO concentration are applied to all

295   reaches.

296   2.3.3   Key factors controlling spatial variability of mean annual NO_3^- removal at basin scale

297   To evaluate the relative importance between hydrologic and substrate variables and modeled

298   NO_3^- removal in the CRB, we used variable importance analysis implemented in a random forest

299   model to identify what factors are associated with the spatial variation of NO_3^- removal amounts

300   (Figure 1). A random forest model was built with the R "randomforest" package using the key

301   input variables and modeled NO_3^- removal amounts (kgN/m^2/day), with 80% of samples used to

302   train the random forest model and 20% used to test the model prediction. We used the R^2 and

303   mean squared error (MSE) to quantify the model prediction accuracy.

304   The random forest model we developed was used to compute the partial dependence of each

305   variable on the modeled NO_3^- removal amount and to measure importance ranks of key input

306   variables. We tested whether the ranks of variable importance vary across the reaches with

307   different sizes and land uses. To measure the importance of key variables in the random forest

308   model, we used Gini impurity measures to determine how well each tree is classified and the

309   variance within each tree. Lower variance represents better classification of each variable. Also,

310   to generalize which watershed and stream properties can better represent the spatial variation of

311   HZ NO_3^- removal amount in the CRB, we developed a random forest model with publicly

312   available watershed/stream variables (Figure 1 and Table 1). The detailed information for each

313   variable used in the random forest model is found in the supporting information (Table S4). The

314   watershed and stream properties are based on the NHDPLUS database (Schwarz et al., 2018).

315

316   **3.   Results**

317   **3.1 Variation of hydrologic variability and substrate availability**

318   We computed the distribution of key model inputs of hydrologic/substrate variables in the

319   reaches across orders and dominant land uses (Figure 4). In the following, we summarize our

320 results, starting with the role of stream size and concluding with land use. Note that we excluded

321 data for 9th order reaches given the small sample (only five).

322   The inputs consistently vary with stream orders (Figure 4a-e). For example, for hyporheic

323 exchange flux, the median flux increased from 1st to 5th order streams and decreased from 6th to

324 8th order rivers. Median residence time increased from 1st to 8th. In contrast, median stream NO_3^-

325 concentrations did not display an obvious trend with channel size. For stream DOC and DO

326 concentrations, the median values increased with stream order, while lower order streams had

327 larger variation of DOC concentration than higher order streams/rivers.

328   When considering land use, reaches in the forest land tended to have the highest hyporheic

329 exchange fluxes, while those in the shrub land had the lowest values (Figure 5). For residence

330 time, reaches in the shrub land had the longest residence time, while forest reaches had the

331 shortest residence time. This is likely explained by the strong correlation between elevation and

332 the drivers for hyporheic exchange. For substrate availability, reaches in the forest and shrub

333 lands had relatively lower stream DOC and NO_3^- but higher DO concentrations than the reaches

334 in the urban and agricultural lands. Reaches in the agricultural lands had the highest DOC and

335 NO_3^-. The reaches in the forest land had the highest DO concentration, but those in the urban

336 land had the lowest DO concentration.

337   We also created the seasonal substrate concentration products, where the spatial patterns of

338 the seasonal DOC do not change with the stream orders (Figure S2); for example, stream DOC

339 increased with the stream orders. However, the relationship between stream DO and stream

340 orders changed with the season. The median of the spring and summer DO concentrations did

341 not vary with the stream orders, but the fall DO concentration decreased with the stream orders

342 and winter DO concentrations increased. On the other hand, the effect of land use on seasonal

343 DOC and DO was minor (Figure S3). For example, while reaches in forest and shrub lands had

344 lower DOC than those in urban and agricultural lands for all seasons, reaches in the agriculture

345 land had the highest DOC concentration, except for winter when urban reaches had the highest

346 DOC. Similarly, spatial patterns of stream DO with different land use did not vary with season.

347 **3.2 Spatial variation of hyporheic zone NO_3^- removal amounts via different flow paths**

348   We computed the mean annual HZ NO_3^- removal amount (kgN/m^2/day) via vertical and

349 lateral hyporheic exchange, respectively (Figure 6). The spatial variations of HZ NO_3^- removal

350   were similar; the spatial correlation (as measured by the Spearman correlation coefficient)

351   between the two estimates was 0.85. The vertical HZ NO_3^- removal was about one order of

352   magnitude higher than the lateral HZ NO_3^- removal. The vertical HZ NO_3^- removal ranged from 0

353   to 0.33 kg N/m^2/day and its mean value was 0.00032 kg N/m^2/day, while the lateral HZ NO_3^-

354   removal ranged from 0 to 0.00517 kg N/m^2/day and its mean value was 2.25e$^{-0.5}$ kg N/m^2/day.

355   The ratio of vertical HZ NO_3^- removal to the total HZ NO_3^- removal ranged from 0.001 to 0.99,

356   with a mean of about 0.78. The ratio increased with the stream orders. For example, median

357   ratios of the 1st and 2nd order streams were about 0.67 and 0.83, respectively, and the median

358   ratio of higher order rivers (> 5th) was close to 1. This result suggests that the HZ NO_3^- removal

359   tends to be more dominated by the vertical exchange in higher order streams and rivers. This is

360   consistent with the modeling results from Gomez-Velez et al. (2015), where the potential

361   denitrification (measured by the reaction significant factor) was higher via vertical hyporheic

362   exchange than via lateral hyporheic exchange in the Mississippi River Basin.

3.3 Spatial variation of hyporheic zone NO_3^- removal amounts in reaches with different
363
orders and land uses
364

365   We quantified the HZ NO_3^- removal amount (kgN/m^2/day) across the reaches with different

366   orders and land uses (Figures 7, S4, and S5). Modeled NO_3^- removal amounts have an unimodal

367   function of stream/river orders (or sizes); medium-sized rivers (4th–6th orders) had the highest

368   NO_3^- removal amounts (Figure 7a). Among the reaches with different land uses, forest reaches

369   have the largest NO_3^- removal amounts (Figure 7b), urban reaches have the second largest, and

370   shrub reaches have the least NO_3^- removal amounts. Their differences were all statistically

371   significant when using the Kruskal-Wallis test, and the *p*-value of the two tests were all less than

372   2.2e-16. We also tested the impact of seasonal substrate concentrations on the spatial variation of

373   NO_3^- removal amounts (Figures S4 and S5). Using seasonal substrate concentration does not

374   change the spatial relationship between modeled HZ NO_3^- removal amounts and stream/river

375   orders; for example, medium-sized rivers still had the largest NO_3^- removal amounts with

376   different seasonal substrate concentrations (Figure S4). However, with seasonal concentrations,

377   rank of the HZ NO_3^- removal amounts changes with different land uses; for example, urban

378   reaches had the largest NO_3^- removal amounts with fall substrate concentrations, while forest

379 reaches had the largest NO_3^- removal amounts in spring. The difference of forest and urban

380 reaches in NO_3^- removal amounts were not statistically significant in summer and winter.

381 **3.4 Influence factors on spatial variation of hyporheic zone NO_3^- removal amounts**

382 To identify the factors that play a dominant role in the spatial variations of the HZ NO_3^-

383 removal, we developed a random forest model with the inputs and HZ NO_3^- removal amounts.

384 The partial dependence plots (Figure S6) showed that stream DOC, residence time, and exchange

385 flux had strong nonlinear relationships with the modeled NO_3^- removal across different sized

386 streams and rivers. Modeled NO_3^- removal increased with stream DOC and exchange flux, but it

387 decreased with residence time. For reaches with different dominant land uses, exchange flux and

388 residence time had a strong positive and negative relationship with the HZ NO_3^- removal

389 amounts, respectively. For all reaches, stream DOC had a high positive nonlinear relationship

390 with the HZ NO_3^- removal amounts, while stream NO_3^- and DO had a weak nonlinear

391 relationship.

392 The variable importance analysis using our random forest model showed that hydrologic

393 variables were more important in explaining HZ NO_3^- removal amount spatial variation than

394 substrate variables (Figure 8). Among the hydrological variables, hyporheic exchange flux was

395 the most important variable and residence time was second most important in all sizes of reaches.

396 Among the substrate variables, stream DOC was the most important. Similarly, the hyporheic

397 exchange flux and residence time were the most and second most important variables for reaches

398 with different land uses, respectively. While residence time was always the second most

399 important variable across the reaches with different land uses, among the substrate variables, the

400 stream DOC was the most important in all reaches except for the shrub reaches. For the shrub

401 reaches, the stream NO_3^- showed higher importance than the stream DOC.

402 We evaluated the impact of substrate availability on the HZ NO_3^- removal amount in reaches

403 across the different sizes and land uses (Figure 9). On average, removing substrate concentration

404 limits tended to increase HZ NO_3^- removal amounts. Among substrate availability, applying the

405 maximum DOC concentrations most increased the HZ NO_3^- removal for all sized reaches and

406 with different land uses, while maximum NO_3^- concentrations least increased HZ NO_3^- removal

407 amounts. Among the reaches with different land uses, shrub reaches showed the largest increase

408   in HZ NO_3^- removal by removing DOC limits. Agricultural reaches showed the least increase by
409   removing the substrate limits. Among the different sized reaches, small streams showed the
410   largest increases in HZ NO_3^- removal amount. This result suggests that stream DOC is the most
411   limiting substrate to NO_3^- removal, especially for the reaches with relatively lower DOC
412   concentrations (Figures 4 and 5).

413   **3.5 Relationship between watershed/stream characteristics and NO_3^- removal amounts**

414   With the publicly available watershed and stream properties data, we developed another
415   random forest model to predict the HZ NO_3^- removal amounts in the CRB to generalize which
416   watershed/stream characteristics can better explain the spatial variation of the HZ denitrification.
417   We built random forest models using the HZ NO_3^- removal amounts via vertical, lateral, and total
418   hyporheic exchange, respectively. Each model showed high predictive accuracy, with R^2 values
419   greater than 0.96 and MSE values less than 0.06 (Figure 10a and Table 2). The variable
420   importance plots showed that for the lateral NO_3^- removal amounts, D50, annual precipitation,
421   annual evapotranspiration, and stream slope were the most important variables (Figure 10b);
422   while for vertical NO_3^- removal amounts, D50, annual precipitation, annual evapotranspiration,
423   vegetation index, and percent of shrub area were the most important variables (Figure 10c). For
424   total NO_3^- removal amounts, D50, annual precipitation, annual evapotranspiration, and percent of
425   shrub area were the most important variables (Figure 10d). The D50, stream slope variables, and
426   annual precipitation were highly associated with the hyporheic exchange rate since the variables
427   were used to calculate streambed hydraulic conductivity in NEXSS (Gomez-Velez et al., 2015).
428   The percent of shrub area was a key predictor in estimating stream DOC concentrations
429   (Figures 4 and S9). The results of variable importance supported that the HZ NO_3^- removal
430   amount increased with hyporheic exchange flux, which positively correlated with streambed
431   hydraulic conductivity (or D50). The modeled NO_3^- removal was also sensitive to the available
432   DOC concentrations, which was negatively correlated to the percent of shrub area. To test how
433   well our random forest model can be applied to the sub-basin in the CRB, we also built a random
434   forest model with the same input data. As with the CRB, the most important variable for each
435   sub-basin was all D50 (Figure S10), and the second most influential variable was mean annual
436   precipitation or basin area, or bankfull width, depending on sub-basins.

437

4. Discussion

4.1 Key controls on spatial hyporheic zone denitrification variations

This study used the basin-scale RCM and random forest models to identify key factors associated with spatial variation of HZ denitrification in the CRB. Results showed that hydrologic variables were more important than substrate variables in explaining the spatial variation of HZ denitrification in reaches across different sizes and land uses. Among the selected hydrologic variables, hyporheic exchange flux was the most important variable for all reaches with different sizes and land uses. Among the substrate variables, stream DOC was considered the most important. Previous studies showed hydrologic variables can explain HZ denitrification. For example, the annual runoff variable can explain 91% of nitrogen attenuation from 49 watersheds in northwestern France among 13 biogeochemical and 12 hydrologic proxies (Frei et al., 2020). The stream depth was used to explain in-stream nitrogen loss rates in many studies (Alexander et al., 2000). The residence time and exchange flux or its combination were used to explain the potential denitrification capacity in different river basins (Gomez-Velez et al., 2015; Gomez-Velez & Harvey, 2014; Harvey et al., 2019). The importance of stream DOC in regulating HZ denitrification has been highlighted previously. Zarnetske et al. (2011) showed that labile DOC limits the HZ denitrification through reach-scale experiments. Also, Jan et al. (2021) showed through numerical experiments at the watershed scale that DOC was a limiting factor when exchange flux becomes higher and stream nitrate concentration was less sensitive, which is similar to the substrate sensitivity analysis result (Figure 9). Hester et al. (2014) showed that surface DOC, groundwater NO_3^-, and hydraulic conductivity of streambeds were the most sensitive parameters affecting the HZ denitrification through numerical experiments.

Among the different sized reaches, medium rivers (4th–6th orders) had the highest denitrification due to the largest exchange flux. The literature shows mixed results in the effects of reach size on denitrification (Alexander et al., 2007, 2009; Tank et al., 2008; Wollheim et al., 2006). In our modeling, the highest exchange flux in the medium-sized rivers was mainly due to the coarser grain size (or higher hydraulic conductivity) of the streambed sediment. While the stream DOC, which limits denitrification, increased with stream orders (or sizes) in the CRB (Figures 4 and S2), the spatial pattern of hyporheic exchange flux controlled the relationship between denitrification amounts and reach sizes. The potential difference between studies may

468   be due to the spatial variation of sediment hydraulic conductivity along the different reach sizes

469   between the river basins if the effect of substrate availability has less influence on denitrification

470   than hydrologic variables. Also, our modeling study showed that hydrologic variables were more

471   important in determining the spatial variation of denitrification in the stream networks than

472   substrate variability. Thus, the hyporheic exchange attributed to the streambed hydraulic

473   properties determined the effect of reach sizes.

474   Among the four dominant land use types, forest reaches had the highest HZ denitrification

475   due to the highest hyporheic exchange flux (Figure 5b). The urban reaches had the second largest

476   denitrification. However, the rank in difference of forest and urban reaches in HZ denitrification

477   vary with seasonal substrate concentrations; for example, in fall, urban reaches had larger

478   denitrification than forest reaches. Therefore, the substrate concentration can be important in the

479   denitrification process, especially for the forest reaches where the denitrification is limited by

480   sources rather than transport.

481   Agricultural reaches had the largest DOC and NO_3^- and the second lowest DO concentration.

482   These reaches, however, were characterized by lower denitrification than forest and urban

483   reaches. Lower denitrification in the agricultural reaches was mainly due to lower exchange flux.

484   Shrub reaches showed the lowest exchange flux and substrate concentration, so they had the

485   lowest denitrification amounts. This limiting factor on HZ denitrification in streams with

486   different land uses is consistent with the result of Myers (2008), who showed that among nine

487   streams in western Wyoming, agriculture and forest reaches had the lowest and highest exchange

488   fluxes, respectively, while agricultural reaches had higher DOC and NO_3^- concentrations than

489   forest reaches. However, the agricultural reaches showed the highest denitrification due to

490   highest substrate availability (e.g., organic matters) in the hyporheic sediments, even though the

491   modeled exchange flux was the lowest in the agricultural reaches. Also, a study by Mulholland et

492   al. (2008), using data from nitrogen stable isotope tracer experiments across 72 streams and eight

493   regions, obtained results that contrast with ours, i.e., urban streams had the highest denitrification

494   rate, while agricultural streams had the second largest denitrification rate, and forest streams had

495   the lowest denitrification rate.

496   Our modeling study showed that agricultural reaches had lower denitrification than urban and

497   forest reaches due to the lowest hyporheic exchange. Interestingly, the two studies showed

498   opposite results, even though they shared the same limiting factor on denitrification in

499   agricultural and forest reaches. The differences can be explained by the representative time scale

500   implicit in our model, which represents long-term average conditions. The experimental study of

501   Myers (2008), on the other hand, represents short-term conditions. Similarly, the difference in

502   both substrate concentration and exchange flux between reaches with different land uses may

503   determine denitrification. In our modeling study, while forest reaches showed the largest

504   denitrification in most scenarios, in fall the urban reaches showed higher denitrification than

505   forest reaches when the highest DOC concentration was observed. Therefore, our modeling

506   results suggest that the combination of substrate concentration and hydrologic exchange

507   determine the difference of HZ denitrification in the reaches with different land uses.

508   **4.2 Generalization of important watershed/stream variables in controlling HZ**

509   **denitrification**

510   This study used a machine-learning approach (i.e., random forest model) to improve our

511   understanding of which watershed/stream variables can better explain the spatial variation of HZ

512   denitrification in the CRB. This approach is a powerful tool to predict complex systems, but due

513   to low interpretability, machine learning is considered a box model. However, our modeling

514   study demonstrated that our random forest models successfully captured sub-basin/basin-scale

515   modeled denitrification, and the selected important variables all represented the dominant

516   processes that controlled denitrification across streams with different sizes and land uses.

517   Our random forest model showed very high prediction accuracies; R^2 values are greater than

518   0.96 and MSE values are less than 0.06. This result suggests that the random forest model with

519   publicly available watershed and stream properties data can capture key variables controlling

520   basin-scale spatial denitrification variation, even though there are complex interactions between

521   many processes/variables determining the spatial variation of HZ denitrification.

522   Also, the variable importance analysis showed that the stream morphological parameters

523   (D50 and stream slope), climate (annual precipitation and evapotranspiration), and stream DOC

524   (percent of shrub area) can explain most HZ denitrification variability. D50 and stream slope

525   were highly correlated with the modeled exchange flux used in this study. The percent of shrub

526   area was one of two predictor variables in stream DOC concentration, which was a major

527   limiting substrate concentration in the modeled denitrification. Our study demonstrates that our

528   random forest model and a small number of key watershed/stream variables (D50, stream slope,

529   precipitation/evapotranspiration, and land cover), which are fairly easy to measure or

530   characterize, can be used to determine the spatial variation of HZ denitrification at the basin

531   scale, without explicit and complex numerical modeling. Therefore, the important variables and

532   random forest model we developed can be used as a hypothesis testing tool for spatial variation

533   of HZ denitrification at the basin scale and as a sampling design tool for large-scale HZ

534   experimental studies.

535   **4.3 Implications for role of hyporheic zone in river corridor processes under future climate**

536   **changes**

537   In the CRB, it is expected that future climate change will increase winter/spring flow,

538   decrease summer flow (Hamlet et al., 2013), and increase stream water temperature (Ficklin et

539   al., 2014). The sensitivity of hydrologic changes to future climate change will also vary between

540   sub-basins in the CRB. This change obviously alters the effectiveness of the HZ in regulating

541   water quality in rivers. Based on our modeling results, denitrification increased with the

542   hyporheic exchange, which was a function of grain sizes of streambed, annual

543   precipitation/evapotranspiration, and stream slope, while lower stream DOC availability may

544   limit denitrification. Compared with other river basins in the United States, the streams of the

545   CRB had lower DOC concentrations (Yang et al., 2017), and watershed DOC processes were

546   characterized as transport-limited rather than source-limited (Zarnetske et al., 2018). Therefore,

547   we expect that increasing runoff can generate higher DOC flux (or concentration) in streams,

548   which may promote denitrification in the HZ.

549   More frequent and intense fires are expected due to future climate conditions (Abatzoglou &

550   Williams, 2016), which can alter the conditions of terrestrial and aquatic systems. For example,

551   fire removes vegetation and delivers more nitrogen/sediments via higher peak flow. On the other

552   hand, fire reduces DOC transport in streams due to biomass and soil carbon burning (Wei et al.,

553   2021). Therefore, higher exchange/more nitrogen availability in the HZ may increase

554   denitrification, while lower sediment hydraulic conductivity values due to finer particle sediment

555   transport by fire and reduced DOC concentrations can reduce denitrification. The impact of fire

556   on HZ denitrification requires extensive future works. Also, the climate and land use changes or

557   their combination may alter the future stream water qualities in different ways (El-Khoury et al.,

558 2015). Therefore, future study should consider both projected changes in determining the role of
559 the HZ.

4.4 Implications for stream/watershed management

561   Excesses in agriculture activity and urbanization continue to degrade water quality in streams
562 and rivers through increases in atmospheric pollutant depositions and excess in nutrient exports
563 (Frei et al., 2020; Le Moal et al., 2019). To improve water quality in rivers, reducing nutrient
564 loading and increasing nutrient removal should be considered. Our modeling study suggests that
565 increasing denitrification occurs by enhancing the exchange flux between stream and HZ. This
566 result is aligned with previous works (Liu & May Chui, 2020; Ward et al., 2011). For example,
567 Liu & May Chui, (2020) demonstrated that through surface and hyporheic flow simulations,
568 increasing hyporheic flux by elevating the height of weirs led to maximizing the nitrogen
569 removal amounts and nitrogen removal ratios. Our modeling also shows that denitrification
570 through vertical exchange is larger than that through lateral exchange and its difference is larger
571 for the large river. This result suggests that enhancing the vertical exchange with higher grain-
572 sized (permeable) streambed materials is more effective in reducing excess nitrogen than lateral
573 exchange through induced channel meandering or others. In addition to enhancing exchange
574 flux, modifying substrate concentration may alter the efficiency of denitrification processes in
575 the HZ. For example, our modeling shows that when exchange flux is high, stream DOC
576 concentration is a limitation factor in the HZ denitrification (Jan et al., 2021). Therefore, to
577 maximize the nitrogen removal process in the HZ, a combination of high exchange flux and
578 stream DOC availability may be required.

4.5 Current research limitations and future study

580   This study demonstrated that combination of the reaction network model and empirical
581 methods can quantify the spatial variation of HZ denitrification at the basin scale. However, due
582 to the simplified model structure and assumptions used, this model had several limitations. The
583 first limitation of this study was that hydrological/substrate variables were assumed to be
584 constant over time, and the variables were empirically estimated or dependent on the other model
585 outputs (e.g., SPARROW flow and total nitrogen fluxes). This assumption may create a bias in a
586 different way depending on hydrologic and substrate conditions. For example, in the streams

587 where hydrologic conditions are unsynchronized or synchronized with substrate variables,

588 modeled denitrification may be overestimated or underestimated with the current model

589 assumptions. Future studies should implement the dynamic hydrologic/substrate concentration

590 in-stream and in the HZ; for example, the SWAT-MRMT-R model (Fang et al., 2020) can be

591 used, and to account for the dynamic hydrologic exchange flux/residence time in the HZ, the

592 SWAT-MODFLOW (Bailey et al., 2016) or other integrated hydrologic–biogeochemistry

593 models (Chen et al., 2020) may be considered.

594   The current model was heavily dependent on the NEXSS-based hyporheic exchange flux and

595 residence time. Even though NEXSS used the physical hydraulic/groundwater models, the

596 exchange flux and residence time were highly correlated with the estimated hydraulic

597 conductivity of the streambed. The NEXSS model used an empirical relationship between D50

598 and sediment hydraulic conductivity to derive the hydraulic conductivity of the streambed at the

599 NHDPLUS stream reach (Gomez-Velez et al., 2015). High spatial heterogeneity of grain size

600 distribution within reach-scale stream sediment (Ren et al., 2020) and its change due to

601 disturbance make it challenging to estimate the representative hydraulic conductivity at the

602 reach-scale (Stewardson et al., 2016). The hydrologic condition also alters vertical distribution of

603 hydraulic conductivity in streambeds; for example, gaining streams have higher conductivity

604 with depth, but losing streams have lower conductivity (X. Chen et al., 2013). Therefore, a future

605 study should focus on introducing advanced methods (i.e., machine learning approaches) and

606 find better predictor variables for streambed hydraulic conductivity (Abimbola et al., 2020) to

607 reduce the uncertainty in the RCM.

608   The second limitation is that this model does not explicitly simulate nitrification processes in

609 the HZ. The current model only implements aerobic respiration and denitrification. When

610 oxygen is abundant and residence time is short, nitrification can be dominant (Zarnetske et al.,

611 2012). This model assumes that nitrification is not dominant. Based on the Dakomber number,

612 lower order streams tend to have lower residence time, so nitrification may be an important

613 process. Interestingly, most streams in the CRB with low residence times tend to have a drainage

614 area with forest lands. Our modeling study suggests that denitrification in the forest streams was

615 mainly limited by the available DOC, but not stream nitrate concentration. Even if nitrate can be

616 more abundant via nitrification because of shorter residence time in the HZ, denitrification of

617 forest streams may not increase because nitrate is not a major limiting factor.

618   The last limitation is that the current model estimates of HZ denitrification are not validated
619   with field measurements, even though the RCM computed the HZ denitrification using the
620   reaction network model with reasonable estimates of hydrologic and substrate variables. This
621   deficiency may reflect the limitation of currently available denitrification measurements for the
622   HZ, especially for large river basins. Many experimental studies focus on total in-stream
623   processes of nutrient uptake rather than exclusively denitrification measurements (Tank et al.,
624   2008; Findlay et al., 2011). Since our model estimates represent spatially varied denitrification
625   and temporally averaged conditions, the comparison with short-term snap measurements that are
626   usually available in the experimental studies is a big challenge. A recent study in the HJ Andrew
627   watershed in Oregon has done the detailed mapping of stream geomorphology, hydrology,
628   biology, and chemistry along the 5th order streams of the forested watershed (Ward et al., 2019).
629   This may be a good starting dataset to validate the model inputs (e.g., concentrations of
630   DOC, DO, and nitrate in the HZ and streambed hydraulic conductivity) and the modeled
631   denitrification along with the stream orders in the future study.
632
633   **5. Summary and Conclusions**
634   The important role of HZ denitrification is well recognized in hydrologic and
635   biogeochemistry communities (Groffman et al., 2009; Harvey & Gooseff, 2015); however,
636   modeling studies quantifying basin-scale HZ denitrification are still limited in current literature.
637   To fill the knowledge gaps, this study used a simplified, spatially fine resolution, basin-scale,
638   coupled-carbon and nitrogen HZ model and random forest models to identify key controls on the
639   spatial variation of HZ denitrification in the CRB. The variable importance analysis
640   demonstrated that hydrologic variables (hyporheic exchange flux and residence time) were more
641   important in explaining the spatial variation of HZ denitrification than substrate variables (stream
642   DOC, nitrate, and DO) across reaches with different sizes and land uses. Among the hydrologic
643   variables, hyporheic exchange flux can explain most spatial variation of the modeled
644   denitrification amounts. Within the substrate variables, the denitrification amount was limited
645   most by the available DOC. Among the different sized reaches, medium rivers (4th–6th orders)
646   with the highest exchange fluxes had the largest denitrification amounts. Among the reaches
647   affected by different land use, forest reaches exhibited the most denitrification due to the highest
648   exchange flux, and urban reaches had the second largest denitrification due to relative high

649   exchange flux and stream DOC. However, ranks in difference between forest and urban reaches

650   in denitrification amounts can change depending on seasonal substrate concentrations. For

651   example, urban reaches with fall substrate concentration showed higher denitrification than

652   forest reaches. These results suggest the combination of hydrologic variability and stream DOC

653   control the spatial difference of HZ denitrification among the reaches with different land uses.

654   Also, while reaches in the agriculture lands had the highest DOC concentrations, the HZ

655   denitrification amounts were second lowest due to lower exchange flux. Reaches in the shrub

656   land had the lowest denitrification due to both the lowest exchange flux and DOC availability.

657   We expanded our efforts to develop a general random forest model to identify key factors

658   associating with the spatial variation of HZ denitrification in the CRB with publicly available

659   watershed and stream properties data. Our random forest model showed a high performance

660   ($R^2 > 0.96$ and MSE < 0.06), with stream morphology parameters (D50), climate (annual

661   precipitation and annual evapotranspiration), and land use (percent of shrub) the most important

662   variables for explaining spatial variation of the modeled HZ denitrification. These results support

663   the relative importance analysis with the model's input variables; hyporheic exchange flux and

664   available DOC concentration were key limiting factors in HZ denitrification variation in the

665   CRB based on our findings. In this study, hyporheic exchange flux was estimated based on the

666   NEXSS simulation (Gomez-Velez et al., 2015), and its flux was highly dependent on streambed

667   sediment grain size/hydraulic conductivity estimates. To reduce the uncertainty of our RCM,

668   future studies should focus on collecting detailed measurements of hydraulic conductivities (Ren

669   et al., 2020; Stewardson et al., 2016) and developing advanced methods characterizing the spatial

670   variation of hydraulic conductivities (Abimbola et al., 2020). In addition, the current model only

671   represented the spatial averaged conditions of HZ denitrification in the CRB, and key model

672   input variables were temporally constant. Therefore, temporal components should be

673   incorporated using integrated hydrologic–biogeochemistry models to accurately represent basin-

674   scale denitrification in the CRB.

675   Overall, this study indicates that the combination of reaction network modeling and empirical

676   substrate concentration models can quantify the spatial variation of HZ denitrification at the

677   basin scale. This modeling framework can be easily applied to the regional and continental scales

678   and can help to understand the role of the HZ across stream networks in large river basins with

679   different hydrologic/geochemical conditions.

680

Appendix – Descriptions of the basin-scale river corridor model

The RCM computes aerobic respiration and two-step denitrification in the HZ at the scale of NHDPLUS stream reaches within the CRB. Figure A1 shows the conceptual diagram of the RCM. Tables A1 and A2 include the three reactions and their associated model parameter values. The model computes at hourly timesteps, but the model key input data—including exchange flux, residence time, and stream solute (DOC, DO, and NO_3^-) concentrations—are constant over time; thus, we should consider that modeled denitrification is a long-term averaged estimate. In addition, each reaction in the HZ and exchange between HZ and stream are vertically and laterally determined independently. This model computes the solute exchange between stream and HZ as expressed in equations A1 and A2. In equation A2, the exchange volume (V) is computed by multiplying exchange flux (q) by the residence time (τ) and stream surface area (width (w)×length (l)). The three reactions are computed by solving the R_1, R_2, and R_3 with the approach proposed by Song et al. (2017), and the associated parameters are obtained from Table 2 in Song et al. (2018).

The following equation is used to calculate the concentration change in the HZ due to the mass exchange between the stream and HZ, as well as microbial reactions in the HZ:

$$\frac{d[C_{i,t}]}{dt} = \frac{1}{\tau}\left([C_{s,i} - [C_{i,t}]\right) + \sum_{j=1}^{3} \mu_j R_j \tag{A1}$$

Where τ is the HZ residence time, $C_{s,i}$ is the stream 'i' solute concentration (DOC, NO_3^-, and DO), $C_{i,t}$ is the hyporheic 'i' solute concentration at the 't' time step. μ_i is the stoichiometric coefficient of solute i in reaction j. R_j is the reaction rate the j-th reaction.

$$\frac{d[C_{i,t}]}{dt}V = V \times \frac{1}{\tau}\left([C_{s,i} - [C_{i,t}]\right) + V \times \sum_{i}^{3} \mu_j R_j \tag{A2}$$

Where V is the hyporheic exchange volume ($q \times w \times l \times \tau$). Using equation A2 can compute the mass exchange between stream and HZ.

$$R_i = e_i r_i^{kin}, \text{i=1,2,3.} \tag{A3}$$

709 $$r_i^{kin} = k_i \frac{a_i}{K_{a_i}+a_i} \times \frac{d_i}{K_{d_i}+d_i}(BM) \qquad (A4)$$

710 $$e_i = \frac{r_i^{kin}}{\sum_i^3 r_i^{kin}} \qquad (A5)$$

711   Where k_i, K_{a_i}, and K_d denote the maximum specific uptake rate of organic carbon, half-

712 saturation constants of the electron acceptors, and half-saturation constants for the electron

713 donors. a_i is the concentration of electron acceptor (mol/L), d_i is the concentration of electron

714 donor (mol/L), and biomass (BM) is the concentration of biomass (mol/L). Reaction rate Ri is

715 computed using unregulated effect (a Monod-type kinetics coefficient (r_i^{kin}) in equation A4, and

716 regulated effects (e_i) in equation A5.

717

730

DATA, CODE AVAILABILITY, AND RESOURCES

732 The model codes/scripts for this study will be made available on this PNNL Gitlab repository at

733 https://gitlab.pnnl.gov/sbrsfa/basin-scale-hyporheic-zone-denitrification-modeling, and the key

734 model inputs/outputs are freely available at https://doi.org/10.5281/zenodo.7152249.

735

References

736

737 Abatzoglou, J. T., & Williams, A. P. (2016). Impact of anthropogenic climate change on wildfire
738   across western US forests. *Proceedings of the National Academy of Sciences of the United*
739   *States of America*, *113*(42), 11770–11775. https://doi.org/10.1073/pnas.1607171113

740 Abimbola, O. P., Mittelstet, A. R., Gilmore, T. E., & Korus, J. T. (2020). Influence of watershed
741   characteristics on streambed hydraulic conductivity across multiple stream orders. *Scientific*
742   *Reports*, *10*(1), 1–10. https://doi.org/10.1038/s41598-020-60658-3

743 Alexander, R. B., Smith, R. A., & Schwarz, G. E. (2000). Effect of stream channel size on the
744   delivery of nitrogen to the Gulf of Mexico. *Nature*, *403*(6771), 758–761.
745   https://doi.org/10.1038/35001562

746 Alexander, R. B., Boyer, E. W., Smith, R. A., Schwarz, G. E., & Moore, R. B. (2007). The role
747   of headwater streams in downstream water quality. *Journal of the American Water*
748   *Resources Association*, *43*(1), 41–59. https://doi.org/10.1111/j.1752-1688.2007.00005.x

749 Alexander, R. B., Böhlke, J. K., Boyer, E. W., David, M. B., Harvey, J. W., Mulholland, P. J., et
750   al. (2009). Dynamic modeling of nitrogen losses in river networks unravels the coupled
751   effects of hydrological and biogeochemical processes. *Biogeochemistry*, *93*(1–2), 91–116.
752   https://doi.org/10.1007/s10533-008-9274-8

753 Bailey, R. T., Wible, T. C., Arabi, M., Records, R. M., & Ditty, J. (2016). Assessing regional-
754   scale spatio-temporal patterns of groundwater–surface water interactions using a coupled
755   SWAT-MODFLOW model. *Hydrological Processes*, *30*(23), 4420–4433.
756   https://doi.org/10.1002/hyp.10933

757 Baker, M. A., & Vervier, P. (2004). Hydrological variability, organic matter supply and
758   denitrification in the Garonne River ecosystem. *Freshwater Biology*, *49*(2), 181–190.
759   https://doi.org/10.1046/j.1365-2426.2003.01175.x

760 Bardini, L., Boano, F., Cardenas, M. B., Revelli, R., & Ridolfi, L. (2012). Nutrient cycling in
761   bedform induced hyporheic zones. *Geochimica et Cosmochimica Acta*, *84*, 47–61.
762   https://doi.org/10.1016/j.gca.2012.01.025

763   Boyer, E. W., Alexander, R. B., Parton, W. J., Li, C., Butterbach-Bahl, K., Donner, S. D., et al.

764   (2006). Modeling denitrification in terrestrial and aquatic ecosystems at regional scales.

765   *Ecological Applications*. https://doi.org/10.1890/1051-

766   0761(2006)016[2123:MDITAA]2.0.CO;2

767   Chen, X., Dong, W., Ou, G., Wang, Z., & Liu, C. (2013). Gaining and losing stream reaches

768   have opposite hydraulic conductivity distribution patterns. *Hydrology and Earth System*

769   *Sciences*, *17*(7), 2569–2579. https://doi.org/10.5194/hess-17-2569-2013

770   Chen, Xingyuan, Lee, R. M., Dwivedi, D., Son, K., Fang, Y., Zhang, X., et al. (2021).

771   Integrating field observations and process-based modeling to predict watershed water

772   quality under environmental perturbations. *Journal of Hydrology*, 125762.

773   https://doi.org/10.1016/j.jhydrol.2020.125762

774   Curie, F., Ducharne, A., Bendjoudi, H., & Billen, G. (2011). Spatialization of denitrification by

775   river corridors in regional-scale watersheds: Case study of the Seine river basin. *Physics*

776   *and Chemistry of the Earth*, *36*(12), 530–538. https://doi.org/10.1016/j.pce.2009.02.004

777   El-Khoury, A., Seidou, O., Lapen, D. R. L., Que, Z., Mohammadian, M., Sunohara, M., &

778   Bahram, D. (2015). Combined impacts of future climate and land use changes on discharge,

779   nitrogen and phosphorus loads for a Canadian river basin. *Journal of Environmental*

780   *Management*, *151*, 76–86. https://doi.org/10.1016/j.jenvman.2014.12.012

781   Ensign, S. H., & Doyle, M. W. (2006). Nutrient spiraling in streams and river networks. *Journal*

782   *of Geophysical Research: Biogeosciences*, *111*(4), 1–13.

783   https://doi.org/10.1029/2005JG000114

784   Fang, Y., Chen, X., Gomez Velez, J., Zhang, X., Duan, Z., Hammond, G. E., et al. (2020). A

785   multirate mass transfer model to represent the interaction of multicomponent

786   biogeochemical processes between surface water and hyporheic zones (SWAT-MRMT-R

787   1.0). *Geoscientific Model Development*, *13*(8), 3553–3569. https://doi.org/10.5194/gmd-13-

788   3553-2020

789   Ficklin, D. L., Barnhart, B. L., Knouft, J. H., Stewart, I. T., Maurer, E. P., Letsinger, S. L., &

Whittaker, G. W. (2014). Climate change and stream temperature projections in the Columbia River basin: Habitat implications of spatial variation in hydrologic drivers. *Hydrology and Earth System Sciences*, *18*(12), 4897–4912. https://doi.org/10.5194/hess-18-4897-2014

Findlay, S. E. G., Mulholland, P. J., Hamilton, S. K., Tank, J. L., Bernot, M. J., Burgin, A. J., et al. (2011). Cross-stream comparison of substrate-specific denitrification potential. *Biogeochemistry*, *104*(1–3), 381–392. https://doi.org/10.1007/s10533-010-9512-8

Fork, M. L., & Heffernan, J. B. (2014). Direct and Indirect Effects of Dissolved Organic Matter Source and Concentration on Denitrification in Northern Florida Rivers. *Ecosystems*, *17*(1), 14–28. https://doi.org/10.1007/s10021-013-9705-9

Frei, R. J., Abbott, B. W., Dupas, R., Gu, S., Gruau, G., Thomas, Z., et al. (2020). Predicting Nutrient Incontinence in the Anthropocene at Watershed Scales. *Frontiers in Environmental Science*, *7*(January), 1–21. https://doi.org/10.3389/fenvs.2019.00200

Gomez-Velez, J. D., & Harvey, J. W. (2014). A hydrogeomorphic river network model predicts where and why hyporheic exchange is important in large basins. *Geophysical Research Letters*, *41*(18), 6403–6412. https://doi.org/10.1002/2014GL061099

Gomez-Velez, J. D., Harvey, J. W., Cardenas, M. B., & Kiel, B. (2015). Denitrification in the Mississippi River network controlled by flow through river bedforms. *Nature Geoscience*, *8*(12), 941–945. https://doi.org/10.1038/ngeo2567

Groffman, P. M., Butterbach-Bahl, K., Fulweiler, R. W., Gold, A. J., Morse, J. L., Stander, E. K., et al. (2009). Challenges to incorporating spatially and temporally explicit phenomena (hotspots and hot moments) in denitrification models. *Biogeochemistry*, *93*(1–2), 49–77. https://doi.org/10.1007/s10533-008-9277-5

Groffman, P. M., Davidson, E. A., & Seitzinger, S. (2009). New approaches to modeling denitrification. *Biogeochemistry*, *93*(1–2), 1–5. https://doi.org/10.1007/s10533-009-9285-0

Hamlet, A. F., Elsner, M. M. G., Mauger, G. S., Lee, S. Y., Tohver, I., & Norheim, R. A. (2013). An overview of the columbia basin climate change scenarios project: Approach, methods,

817   and summary of key results. *Atmosphere - Ocean*, *51*(4), 392–415.

818   https://doi.org/10.1080/07055900.2013.819555

819 Harvey, J., & Gooseff, M. (2015). River corridor science: Hydrologic exchange and ecological

820   consequences from bedforms to basins. *Water Resources Research*, *51*(9), 6893–6922.

821   https://doi.org/10.1002/2015WR017617

822 Harvey, J., Gomez-Velez, J., Schmadel, N., Scott, D., Boyer, E., Alexander, R., et al. (2019).

823   How Hydrologic Connectivity Regulates Water Quality in River Corridors. *Journal of the*

824   *American Water Resources Association*, *55*(2), 369–381. https://doi.org/10.1111/1752-

825   1688.12691

826 Hester, E. T., Young, K. I., & Widdowson, M. A. (2014). Controls on mixing-dependent

827   denitrification in hyporheic zones induced by riverbed dunes: A steady state modeling

828   study. *Water Resources Research*, *50*(11), 9048–9066.

829   https://doi.org/10.1002/2014WR015424

830 Hotchkiss, E. R., Hall, R. O., Sponseller, R. A., Butman, D., Klaminder, J., Laudon, H., et al.

831   (2015). Sources of and processes controlling CO_2 emissions change with the size of streams

832   and rivers. *Nature Geoscience*, *8*(9), 696–699. https://doi.org/10.1038/ngeo2507

833 Jan, A., Coon, E. T., & Painter, S. L. (2021). Toward more mechanistic representations of

834   biogeochemical processes in river networks: Implementation and demonstration of a

835   multiscale model. *Environ. Model. Softw.*, *145*(August), 105166.

836   https://doi.org/10.1016/j.envsoft.2021.105166

837 Kreiling, R. M., Richardson, W. B., Bartsch, L. A., Thoms, M. C., & Christensen, V. G. (2019).

838   Denitrification in the river network of a mixed land use watershed: unpacking the

839   complexities. *Biogeochemistry*, *143*(3), 327–346. https://doi.org/10.1007/s10533-019-

840   00565-6

841 Lee-Cullin, J. A., Zarnetske, J. P., Ruhala, S. S., & Plont, S. (2018). Toward measuring

842   biogeochemistry within the stream-groundwater interface at the network scale: An initial

843   assessment of two spatial sampling strategies. *Limnology and Oceanography: Methods*,

844   *16*(11), 722–733. https://doi.org/10.1002/lom3.10277

845   Li, M., Gao, Y., Qian, W. J., Shi, L., Liu, Y., Nelson, W. C., et al. (2017). Targeted
846   quantification of functional enzyme dynamics in environmental samples for microbially
847   mediated biogeochemical processes. *Environmental Microbiology Reports*, *9*(5), 512–521.
848   https://doi.org/10.1111/1758-2229.12558

849   Liu, S., & May Chui, T. F. (2020). Optimal in-stream structure design through considering
850   nitrogen removal in hyporheic zone. *Water (Switzerland)*, *12*(5).
851   https://doi.org/10.3390/W12051399

852   Le Moal, M., Gascuel-Odoux, C., Ménesguen, A., Souchon, Y., Étrillard, C., Levain, A., et al.
853   (2019). Eutrophication: A new wine in an old bottle? *Science of the Total Environment*,
854   *651*, 1–11. https://doi.org/10.1016/j.scitotenv.2018.09.139

855   Mori, N., Debeljak, B., Škerjanec, M., Simčič, T., Kanduč, T., & Brancelj, A. (2019). Modelling
856   the effects of multiple stressors on respiration and microbial biomass in the hyporheic zone
857   using decision trees. *Water Research*, *149*, 9–20.
858   https://doi.org/10.1016/j.watres.2018.10.093

859   McCabe, G. J., & Wolock, D. M. (2016). Variability and Trends in Runoff Efficiency in the
860   Conterminous United States. *Journal of the American Water Resources Association*, *52*(5),
861   1046–1055. https://doi.org/10.1111/1752-1688.12431

862   Mulholland, P. J., Helton, A. M., Poole, G. C., Hall, R. O., Hamilton, S. K., Peterson, B. J., et al.
863   (2008). Stream denitrification across biomes and its response to anthropogenic nitrate
864   loading. *Nature*, *452*(7184), 202–205. https://doi.org/10.1038/nature06686

865   Pinay, G., Peiffer, S., De Dreuzy, J. R., Krause, S., Hannah, D. M., Fleckenstein, J. H., et al.
866   (2015). Upscaling Nitrogen Removal Capacity from Local Hotspots to Low Stream Orders'
867   Drainage Basins. *Ecosystems*, *18*(6), 1101–1120. https://doi.org/10.1007/s10021-015-9878-
868   5

869   Pinay, G., Bernal, S., Abbott, B. W., Lupon, A., Marti, E., Sabater, F., & Krause, S. (2018).
870   Riparian corridors: A new conceptual framework for assessing nitrogen buffering across

871   biomes. *Front. Environ. Sci.* https://doi.org/10.3389/fenvs.2018.00047

872   Ren, H., Hou, Z., Duan, Z., Song, X., Perkins, W. A., Richmond, M. C., et al. (2020). Spatial
873   Mapping of Riverbed Grain-Size Distribution Using Machine Learning. *Frontiers in Water*,
874   *2*(November), 1–13. https://doi.org/10.3389/frwa.2020.551627

875   Ren, H., Song, X., Fang, Y., Hou, Z. J., & Scheibe, T. D. (2021). Machine Learning Analysis of
876   Hydrologic Exchange Flows and Transit Time Distributions in a Large Regulated River.
877   *Frontiers in Artificial Intelligence*, *4*(April), 1–18. https://doi.org/10.3389/frai.2021.648071

878   Schmadel, N. M., Harvey, J. W., & Schwarz, G. E. (2021). Seasonally dynamic nutrient
879   modeling quantifies storage lags and time-varying reactivity across large river basins.
880   *Environmental Research Letters*, *16*(9), 095004. https://doi.org/10.1088/1748-9326/ac1af4

881   Schwarz, G. E., Jackson, S. E., & Wieczorek, M. E. (2018). Select Attributes for NHDPlus
882   Version 2.1 Reach Catchments and Modified Network Routed Upstream Watersheds for the
883   Conterminous United States. *United States Geological Survey*.
884   https://doi.org/http://dx.doi.org/10.5066/F7765D7V

885   Seitzinger, S., Harrison, J. A., Böhlke, J. K., Bouwman, A. F., Lowrance, R., Peterson, B., et al.
886   (2006). Denitrification across landscapes and waterscapes: A synthesis. *Ecological*
887   *Applications*, *16*(6), 2064–2090. https://doi.org/10.1890/1051-
888   0761(2006)016[2064:DALAWA]2.0.CO;2

889   Song, H.-S., Thomas, D. G., Stegen, J. C., Li, M., Liu, C., Song, X., et al. (2017). Regulation-
890   Structured Dynamic Metabolic Model Provides a Potential Mechanism for Delayed Enzyme
891   Response in Denitrification Process. *Frontiers in Microbiology*, *8*(September), 1–12.
892   https://doi.org/10.3389/fmicb.2017.01866

893   Song, X., Chen, X., Stegen, J., Hammond, G., Song, H. S., Dai, H., et al. (2018). Drought
894   Conditions Maximize the Impact of High-Frequency Flow Variations on Thermal Regimes
895   and Biogeochemical Function in the Hyporheic Zone. *Water Resources Research*, *54*(10),
896   7361–7382. https://doi.org/10.1029/2018WR022586

897   Stewardson, M. J., Datry, T., Lamouroux, N., Pella, H., Thommeret, N., Valette, L., & Grant, S.

898   B. (2016). Variation in reach-scale hydraulic conductivity of streambeds. *Geomorphology*,

899   *259*, 70–80. https://doi.org/10.1016/j.geomorph.2016.02.001

900   Tank, J. L., Rosi-Marshall, E. J., Baker, M. A., & Hall, R. O. (2008). Are rivers just big streams?

901   A pulse method to quantify nitrogen demand in a large river. *Ecology*, *89*(10), 2935–2945.

902   https://doi.org/10.1890/07-1315.1

903   Ward, A. S., Gooseff, M. N., & Johnson, P. A. (2011). How can subsurface modifications to

904   hydraulic conductivity be designed as stream restoration structures? Analysis of Vaux's

905   conceptual models to enhance hyporheic exchange. *Water Resources Research*, *47*(8), 1–13.

906   https://doi.org/10.1029/2010WR010028

907   Ward, A. S., Zarnetske, J. P., Baranov, V., Blaen, P. J., Brekenfeld, N., Chu, R., et al. (2019).

908   Co-located contemporaneous mapping of morphological, hydrological, chemical, and

909   biological conditions in a 5th-order mountain stream network, Oregon, USA. *Earth System*

910   *Science Data*, *11*(4), 1567–1581. https://doi.org/10.5194/essd-11-1567-2019

911   Ward, A. S., Packman, A., Bernal, S., Brekenfeld, N., Drummond, J., Graham, E., et al. (2022).

912   Advancing river corridor science beyond disciplinary boundaries with an inductive

913   approach to catalyse hypothesis generation. *Hydrological Processes*, *36*(4), 1–19.

914   https://doi.org/10.1002/hyp.14540

915   Wei, X., Hayes, D. J., & Fernandez, I. (2021). Fire reduces riverine DOC concentration draining

916   a watershed and alters post-fire DOC recovery patterns. *Environmental Research Letters*,

917   *16*(2). https://doi.org/10.1088/1748-9326/abd7ae

918   Wise, D.R., Anning, D.W., and Miller, O. L. (2019). *Spatially referenced models of streamflow*

919   *and nitrogen, phosphorus, and suspended-sediment transport in streams of the Pacific*

920   *region of United States*. U.S. Geological Survey Scientific Investigations Report 2019-5106.

921   Wollheim, W. M. (2016). *From Headwaters to Rivers to River Networks: Scaling in Stream*

922   *Ecology. Scaling in Stream Ecology. Stream Ecosystems in a Changing Environment*.

923   Elsevier Inc. https://doi.org/10.1016/B978-0-12-405890-3.00008-7

924   Wollheim, Wil M., Vörösmarty, C. J., Peterson, B. J., Seitzinger, S. P., & Hopkinson, C. S.

925 (2006). Relationship between river size and nutrient removal. *Geophysical Research*
926 *Letters*, *33*(6), 2–5. https://doi.org/10.1029/2006GL025845

927 Yang, Q., Zhang, X., Xu, X., & Asrar, G. R. (2017). An analysis of terrestrial and aquatic
928 environmental controls of riverine dissolved organic carbon in the conterminous United
929 States. *Water (Switzerland)*, *9*(6). https://doi.org/10.3390/w9060383

930 Zarnetske, J. P., Haggerty, R., Wondzell, S. M., & Baker, M. A. (2011). Labile dissolved organic
931 carbon supply limits hyporheic denitrification. *J. Geophys. Res. Biogeosciences*, *116*(4).
932 https://doi.org/10.1029/2011JG001730

933 Zarnetske, J. P., Haggerty, R., Wondzell, S. M., Bokil, V. A., & González-Pinzón, R. (2012).
934 Coupled transport and reaction kinetics control the nitrate source-sink function of hyporheic
935 zones. *Water Resources Research*, *48*(11), 1–15. https://doi.org/10.1029/2012WR011894

936 Zarnetske, J. P., Haggerty, R., & Wondzell, S. M. (2015). Coupling multiscale observations to
937 evaluate Hyporheic nitrate removal at the reach scale. *Freshwater Science*, *34*(1), 172–186.
938 https://doi.org/10.1086/680011

939 Zarnetske, J. P., Bouda, M., Abbott, B. W., Saiers, J., & Raymond, P. A. (2018). Generality of
940 Hydrologic Transport Limitation of Watershed Organic Carbon Flux Across Ecoregions of
941 the United States. *Geophysical Research Letters*, *45*(21), 11,702-11,711.
942 https://doi.org/10.1029/2018GL080005

943

944 Table 1. Lists of key watershed/stream characteristics and properties

Properties	Variables
Climate	Precipitation and air temperature
Topography	Elevation, slope, wetness index, and drainage area
Hydrology	Annual flow, baseflow index, potential evapotranspiration, and actual evapotranspiration
Land	Percent of land use/cover types (forest, wetland, agriculture, urban and shrubland), vegetation index
Soil	Hydraulic conductivity of soil and permeability of surface geology, percent of soil texture and organic matter
Stream	D50, sinuosity, contact time and stream slope, bankfull width, and channel depth

945

946 Table 2. Summary of model performance in the developed random forest model

Model	Train		Test	
	R^2	MSE	R^2	MSE
Lateral denitrification	0.96	0.06	0.96	0.05
Vertical denitrification	0.97	0.04	0.97	0.04
Total denitrification	0.97	0.03	0.97	0.03

947

948

949   Table A1. Aerobic respiration and two steps of denitrification reactions

Reaction process		Reaction equations
Aerobic respiration	R_1	$CH_2O + f_1O_2 + \frac{1}{5}(1 - f_1)NH_4^+ \rightarrow f_1CO_2 + \frac{1}{5}(1 - f_1)C_5H_7O_2N + \frac{1}{5}(3 + 2f_1)H_2O + \frac{1}{5}(1 - f_1)H^+$
Denitrification	R_2	$CH_2O + 2f_2NO_3^- + \frac{1}{5}(1 - f_2)NH_4^+$ $\rightarrow f_2NO_2^- + f_2CO_2 + \frac{1}{5}(1 - f_2)C_5H_7O_2N + \frac{1}{5}(3 + 2f_2)H_2O + \frac{1}{5}(1 - f_2)H^+$
	R_3	$CH_2O + \frac{4}{3}f_3NO_2^- + \frac{1}{5}(1 - f_3)NH_4^+$ $\rightarrow \frac{2}{3}f_3N_2 + f_3CO_2 + \frac{1}{5}(1 - f_3)C_5H_7O_2N + \frac{1}{15}(9 + 16f_3)H_2O + \frac{1}{15}(3 + 17H^+)$

950

951   Table A2. Reaction parameter values and initial substrate concentrations

Reaction rates	Parameter	R_1	R_2	R_3
	f_i	1/3×0.65	0.65	0.99
	$k_i \left(\frac{mole}{l,h}\right)$	3×1.17	1.17	0.97
	$K_{d,i}$ (mmole/l)	0.25	0.25	0.25
	$K_{a,i}$(mmole/l)	0.001	0.001	0.004
Hyporheic zone		DOC	NO_3^-	DO
Initial concentrations (mole/l)		6.37e-5	7.92e-5	2.87e-4

952   R_1 is aerobic respiration reaction ($O_2 \rightarrow CO_2$), R_2 ($NO_3^- \rightarrow CO_2$) and R_3 ($NO_2^- \rightarrow CO_2$) are two
953   steps of denitrification reaction

954   Figures
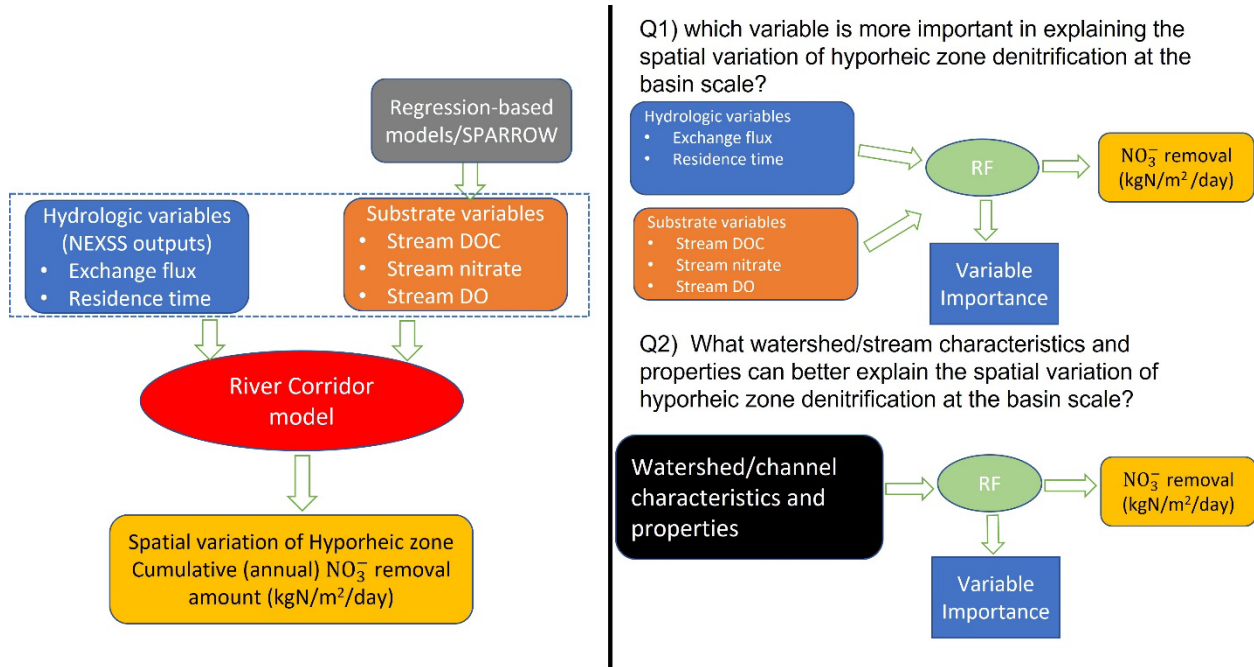
955

956   Figure 1. The framework for studying key factors controlling spatial variation of HZ

957   denitrification in streams across different sizes and land uses in the CRB.

958

959
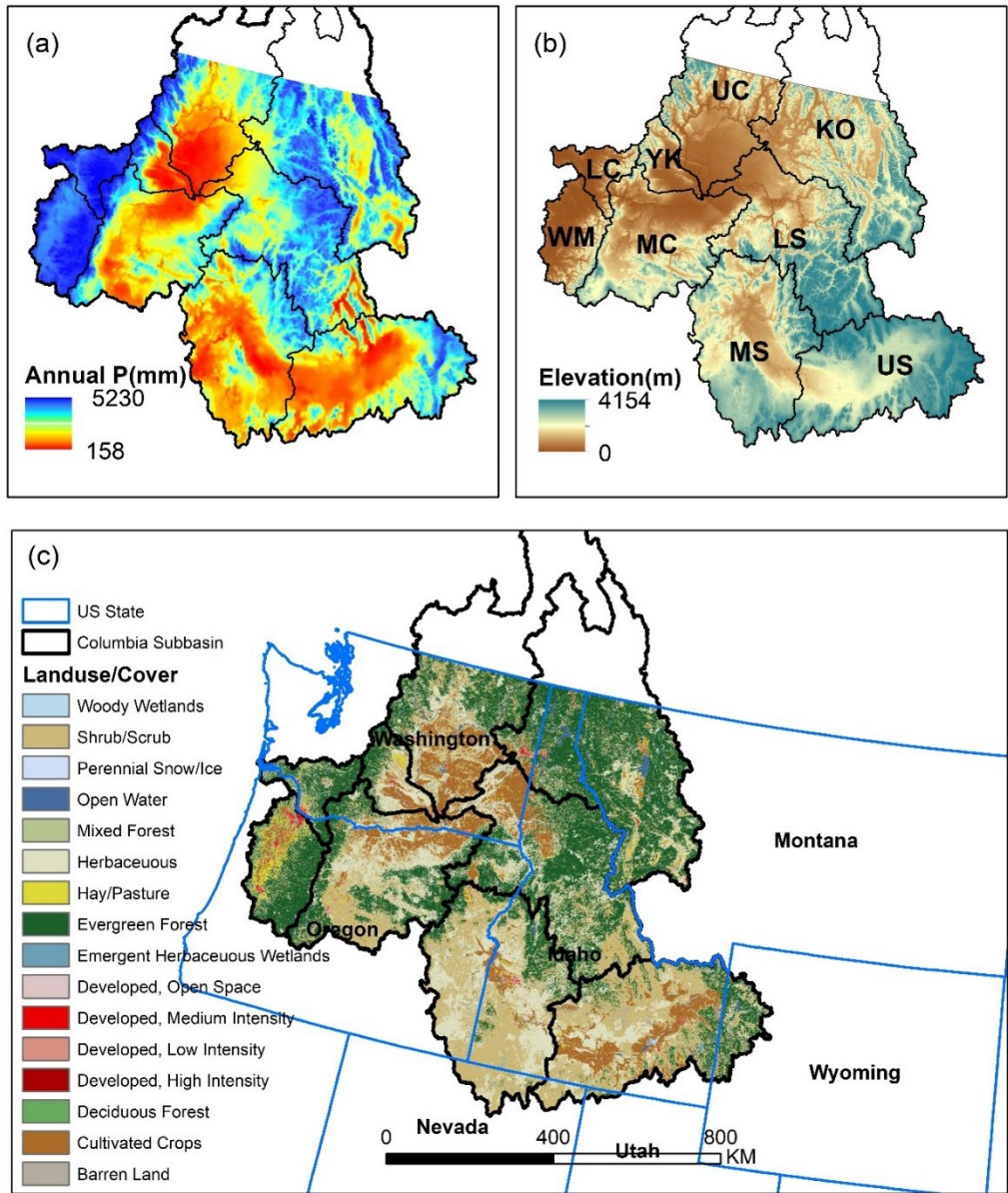
Figure 2. CRB maps: (a) Mean annual precipitation (mm); (b) Elevation and nine major sub-river basins (1) Lower Columbia (LC), (2) Middle Columbia (MC), (3) Upper Columbia (UC), (4) Lower Snake (LS), (5) Middle Snake (MS), (6) Upper Snake (US), (7) Kootenai-Pend Oreille-Spokane (KO), (8) Willamette(WM), and (9) Yakima (YK); and (c) Land use and cover map (National Land Cover Database 2016 data).

965

966
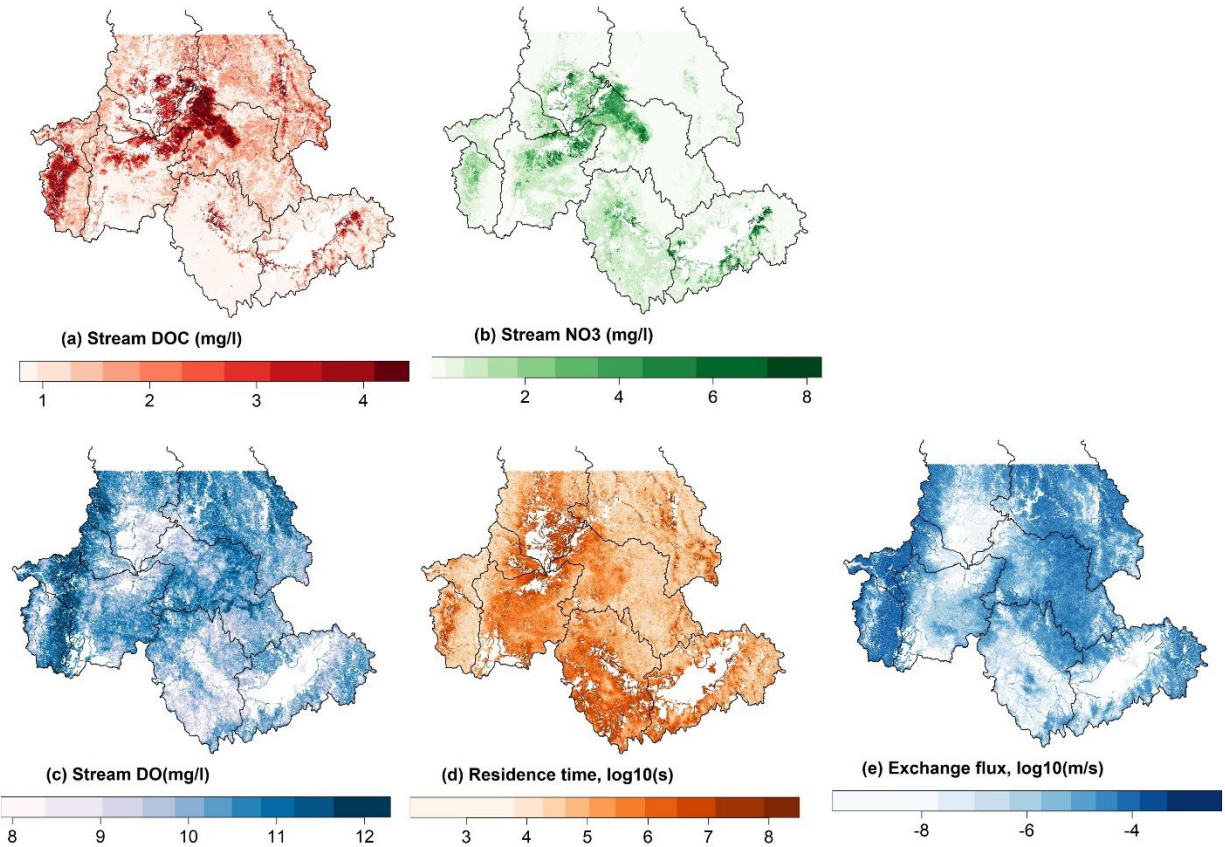
Figure 3. Key input data for the RCM: (a) stream mean annual DOC concentrations (mg/l); (b) stream mean annual NO_3^- concentrations (mg/l); (c) stream mean annual DO concentrations (mg/l); (d) total (lateral and vertical) residence time (log10, second); and (e) total (lateral and vertical) hyporheic exchange flux (log10, m/s).

971
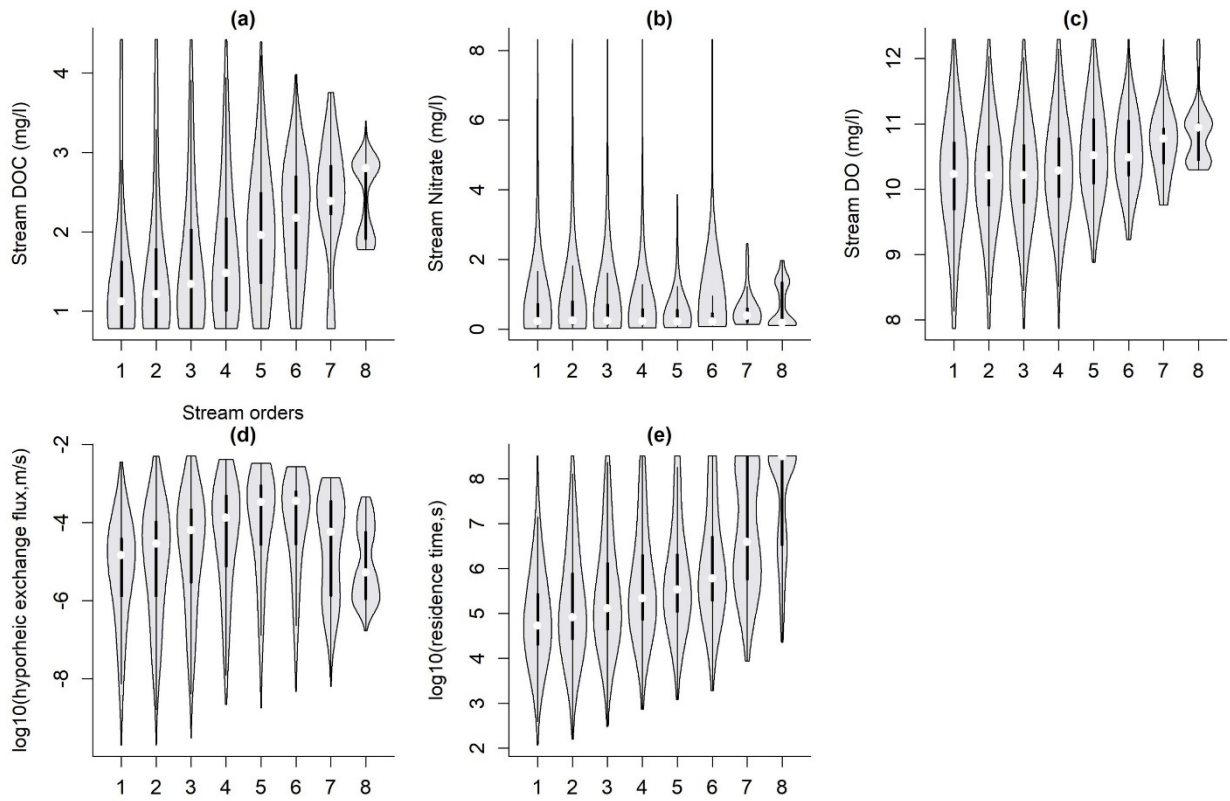
Figure 4. Distribution of key hydrologic and substrate variables in streams with stream orders. In the violine plot, the white point represents median value, the thick black line represents interquartile range (Q1 and Q3), and the thin black lines represent the 1.5×interquantile range.

975
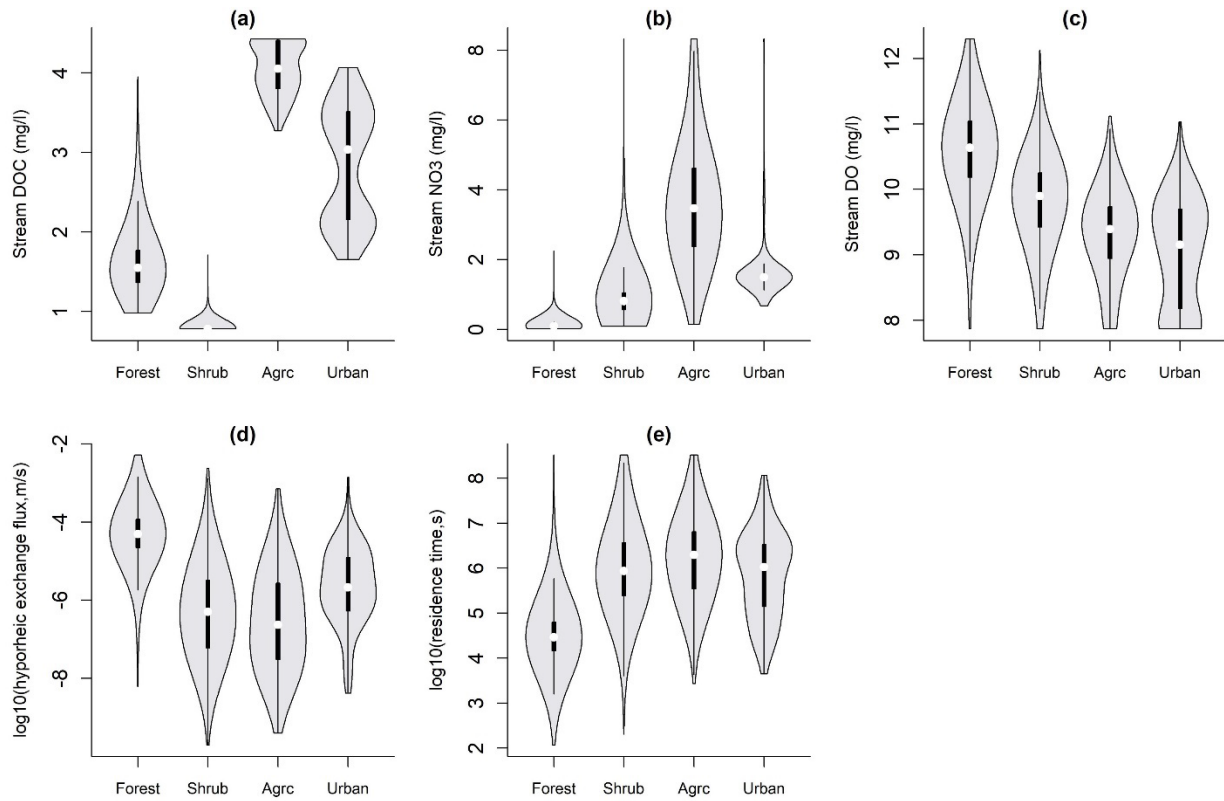
976

977 Figure 5. Distribution of key hydrologic and substrate variables in streams with different land

978 uses. In the violine plot, the white point represents median value, the thick black line represents

979 interquartile range (Q1 and Q3), and the thin black lines represent the 1.5×interquantile range.

980

(a) Lateral NO3 removal amount(log10, kgN/m2/day)

(b) Vertical NO3 removal amount(log10, kgN/m2/day)

(c) Total NO3 removal amount(log10, kgN/m2/day)

(d)

981
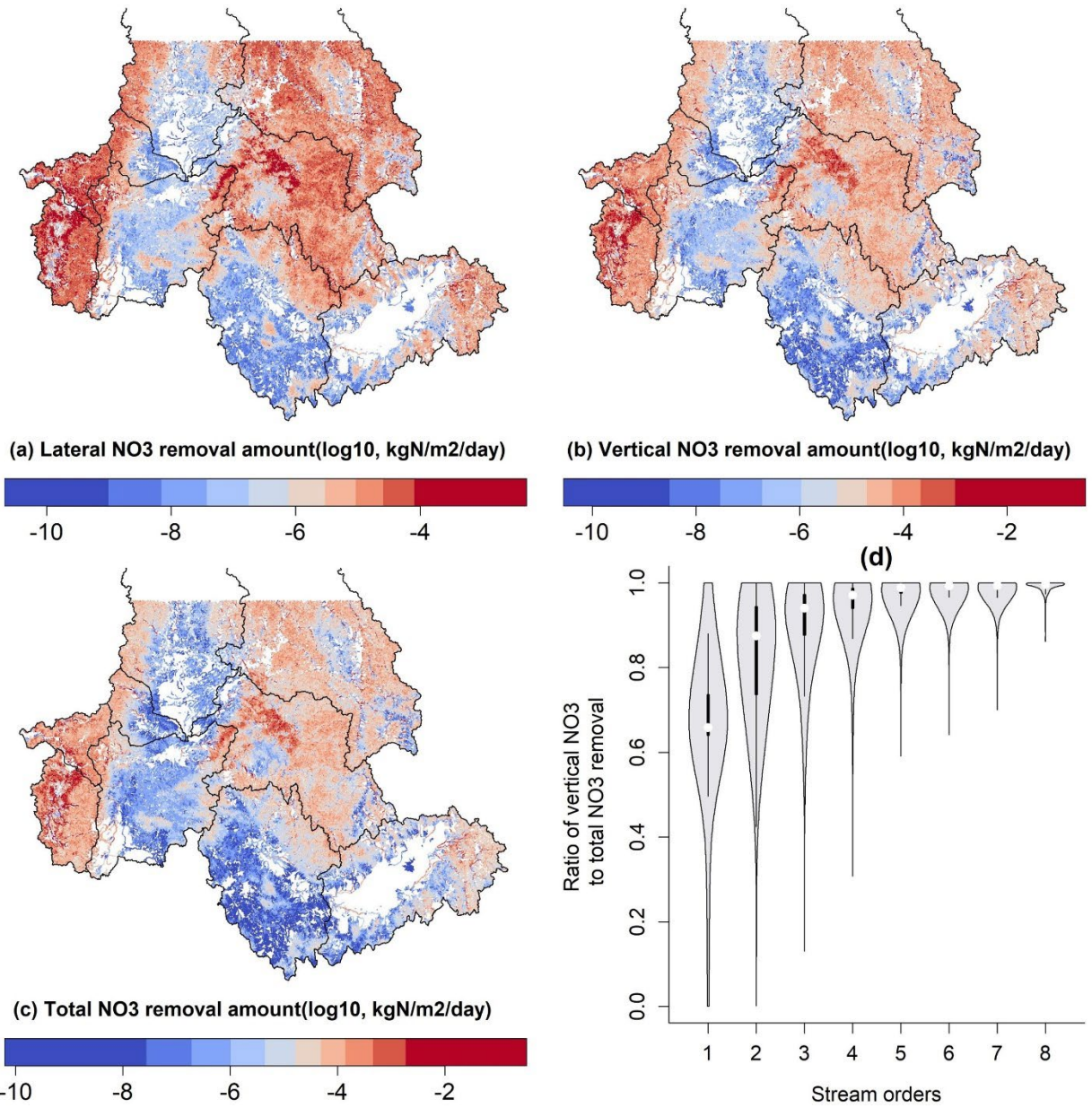
Figure 6. Spatial variation of modeled mean annual HZ NO_3^- removal amount (log10,

kgN/m^2/day): (a) NO_3^- removal amount via lateral hyporheic exchange; (b) NO_3^- removal amount

via vertical hyporheic exchange; (c) NO_3^- removal amount via total hyporheic exchange; (d) ratio

of the vertical NO_3^- removal amount to the total (vertical and lateral) NO_3^- removal amount with

the stream orders.

987

988
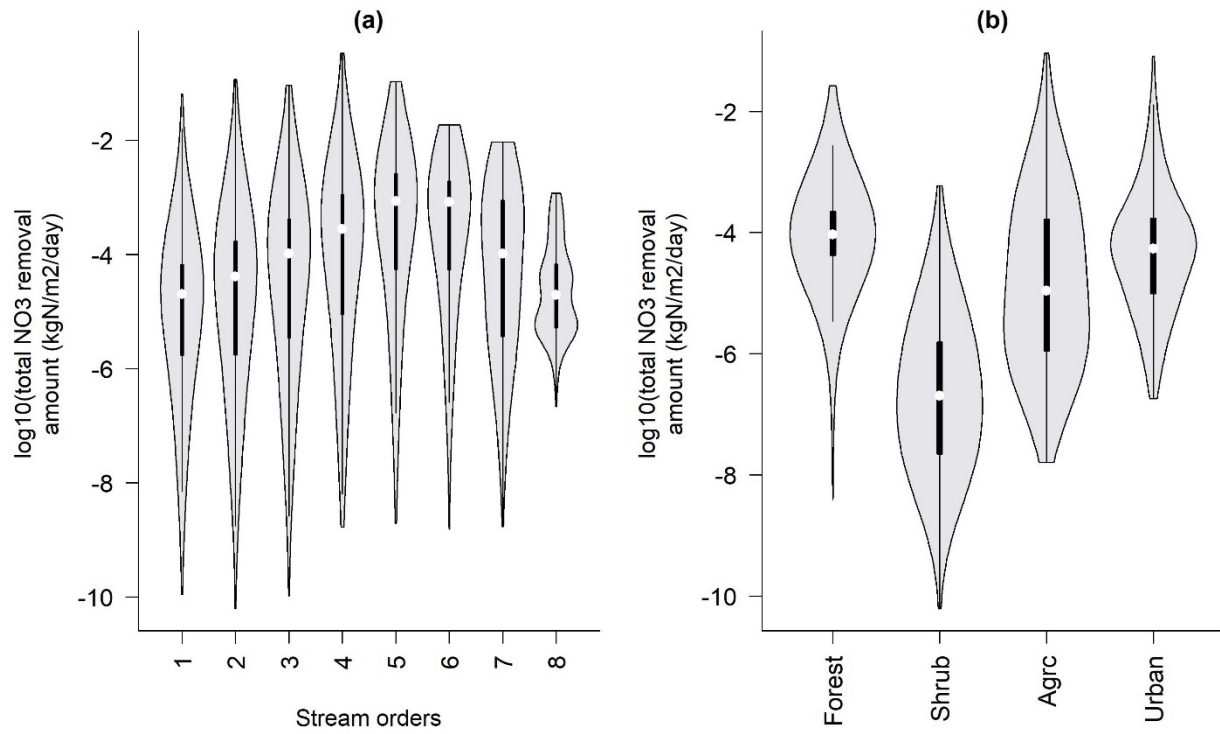
Figure 7. Variation of modeled HZ mean daily NO_3^- removal amount in the reaches with
different orders and land uses: (a) effects of sizes and (b) effects of land use.

991
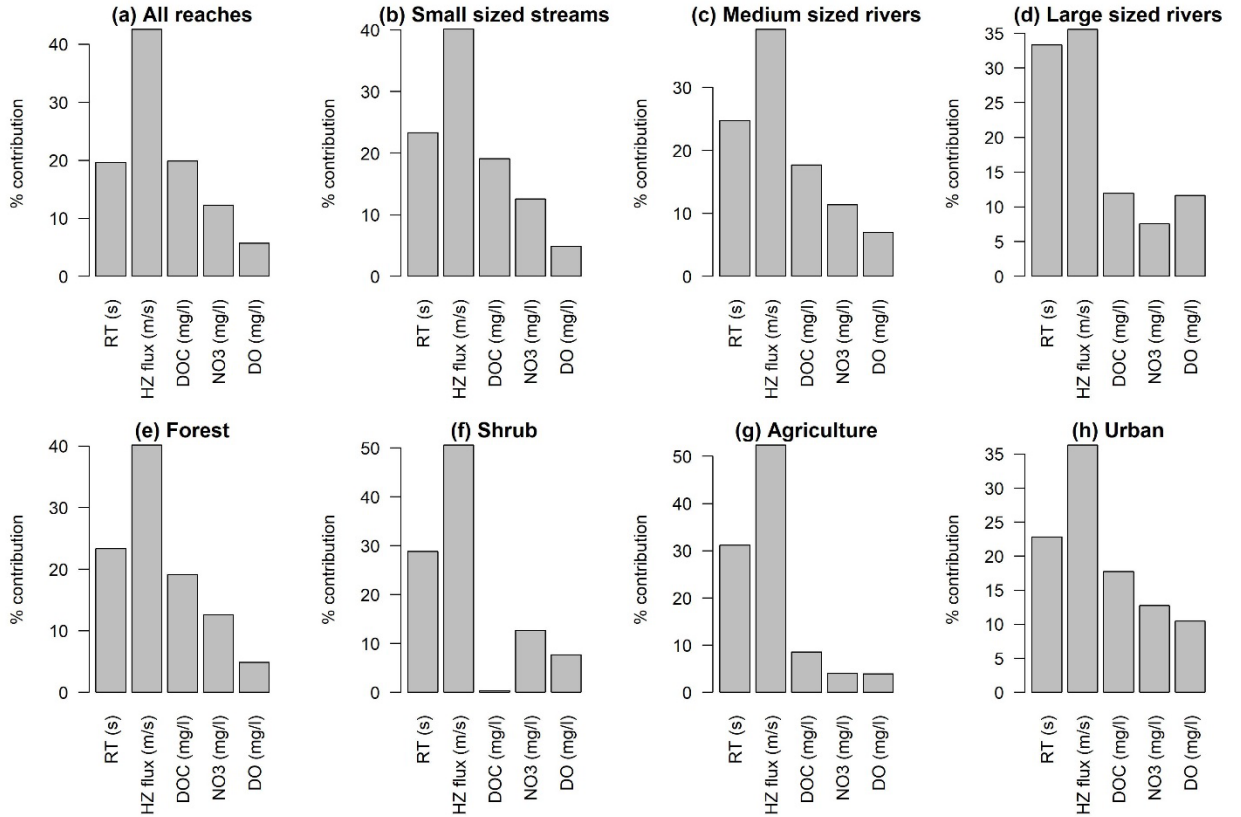
Figure 8. Relative importance of hydrologic variability and substrate availability in controlling spatial variation of the HZ NO_3^- removal amount in reaches along different sizes and dominant land uses. The variable importance (measured by Ginni value) is normalized to calculate the relative importance value (percent contribution) that ranges from 0 to 100.

998
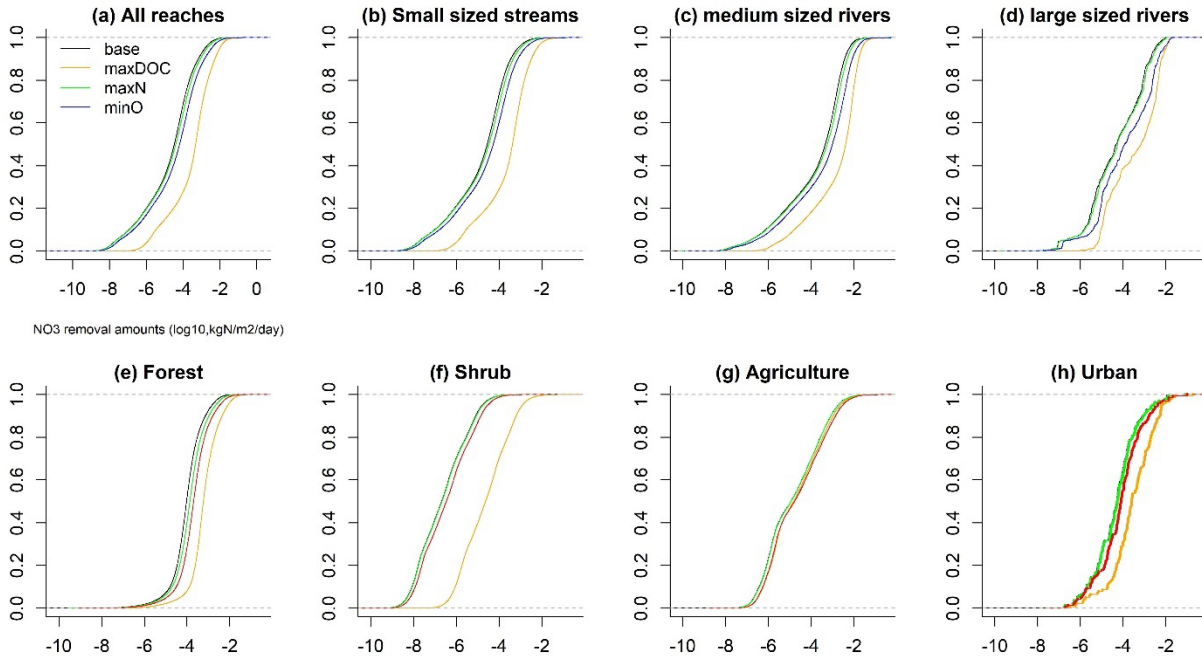
Figure 9. Sensitivity of modeled NO_3^- removal amount (log10(kgN/m^2/day)) to the available substrate concentrations across reaches with different sizes and land uses: (a) all reaches; (b) small streams; (c) medium rivers; (d) large rivers; (e) forest; (f) shrub; (g) agriculture; and (h) urban. The base scenarios used the modeled substrate concentration data (Figure 3a, b, c). The maxDOC scenarios applied a maximum concentration of modeled DOC (Figure 3a) to all reaches, and the maxN scenario applied a maximum concentration of modeled NO_3^- (Figure 3b) to all reaches, and the minO scenarios applied a minimum concentration of modeled DO (Figure 3c) to all reaches.

1007
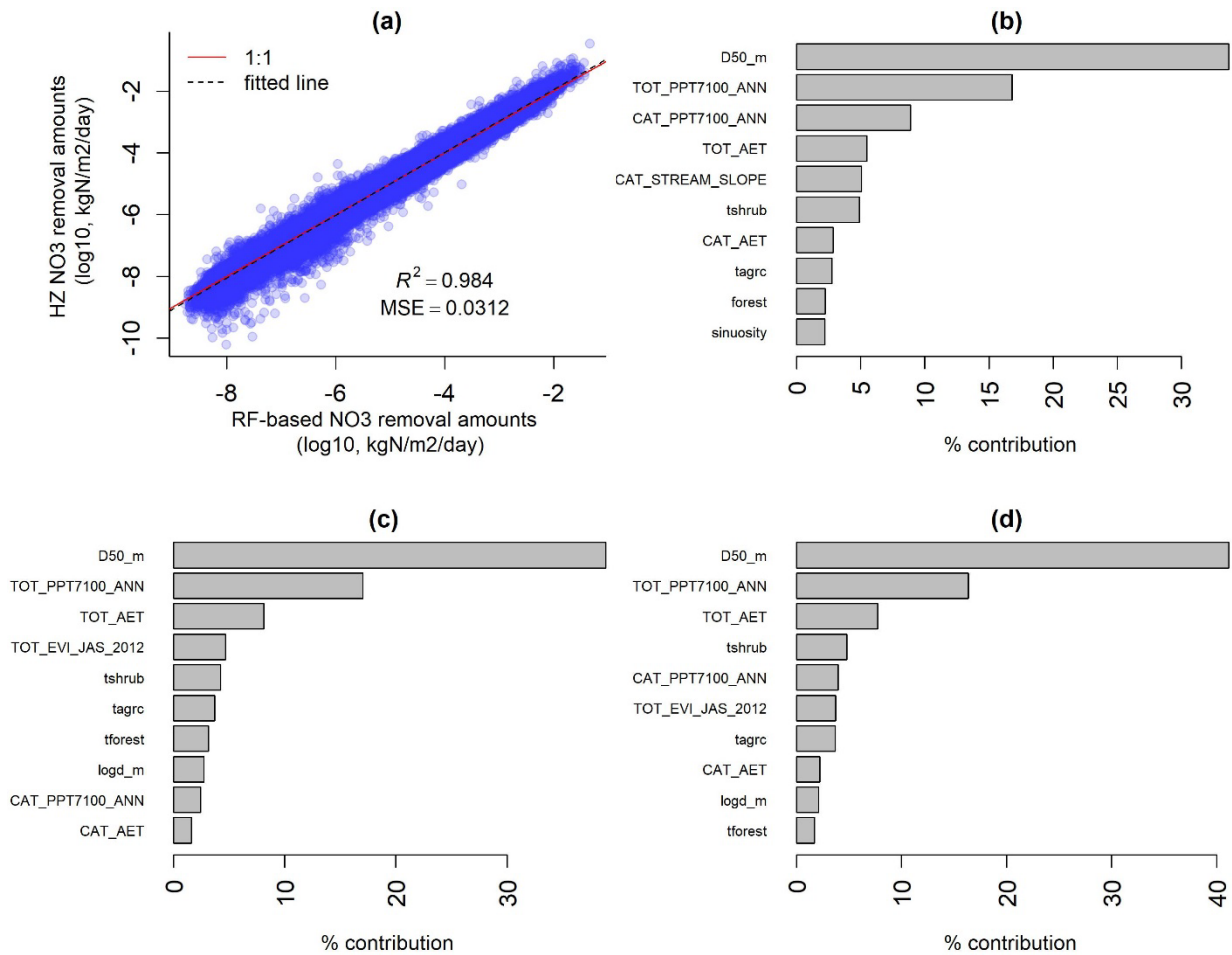
1008

Figure 10. Predictions of the random forest model in the testing period and variable importance analysis results: (a) test results for the total HZ NO_3^- removal amount; (b) top 10 importance variables for lateral NO_3^- removal amount (kgN/m^2/day); (c) top 10 important variables for modeled vertical NO_3^- removal amount (kgN/m^2/day); and (d) top 10 important variables for modeled total NO_3^- removal amount (kgN/m^2/day). The top 10 variables are D50_m (median grain size), TOT_PPT7100_ANN (30-year mean annual precipitation at the NHD cumulated drainage), CAT_PPT7100_ANN (30-year mean annual precipitation at the NHD catchment), TOT_AET (mean annual evapotranspiration at the NHD cumulated drainage), CAT_AET (mean annual evapotranspiration at the NHD catchment), tshrub (percent of shrub land at the NHD cumulated drainage area), TOT_EVI_JAS_2012 (vegetation index at the NHD cumulated drainage area), CAT_STREAM_SLOPE (stream slope at the NHD catchment), tforest (percent of forest land at the NHD cumulated drainage), forest (percent of forest land at the NHD

1021   catchment), tagrc (percent of agricultural land at the NHD cumulated drainage), logd_m

1022   (log10(stream depth.,m)), and sinuosity (stream sinuosity).

1023
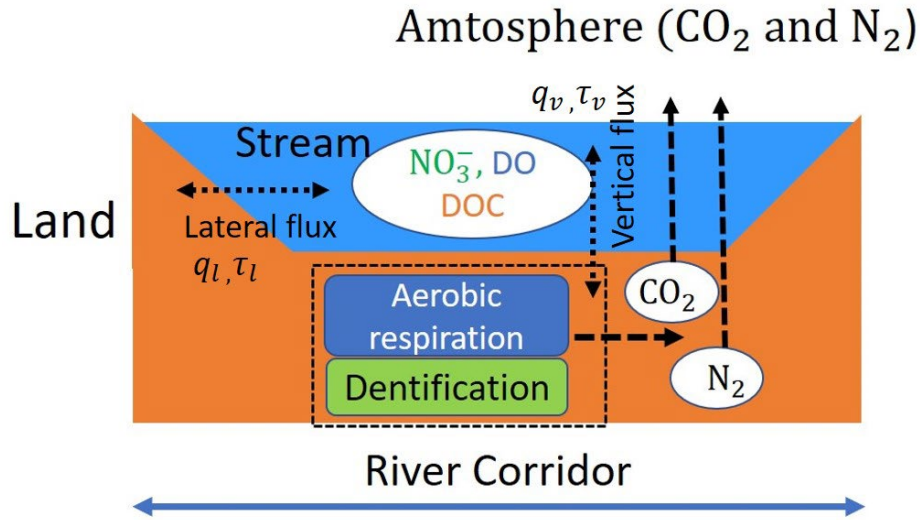
1024

1025   Figure A1. Simplified conceptual diagram of the RCM. The RCM computes the aerobic

1026   respiration and two-step denitrification in the HZ at the reach scale. The model requires five key

1027   inputs; stream DOC and DO were estimated by the two regression models, and stream NO_3^-

1028   concentrations were estimated from the SPARROW 2012 model (Wise et al., 2019), and the

1029   vertical and lateral exchange fluxes (q_v, q_l) and their median residence times (τ_v, τ_l) between

1030   the streams and HZ were estimated from NEXSS (Gomez-Velez et al., 2015).

1031